minerals

MDPI

Article

Highly Metalliferous Potential of Framboidal and Nodular Pyrite Varieties from the Oil-Bearing Jurassic Bazhenov Formation, Western Siberia

Kirill S. Ivanov [1,*], Valery V. Maslennikov [2], Dmitry A. Artemyev [2,3] and Aleksandr S. Tseluiko [2]

[1] Institute of Geology and Geochemistry, Ural Branch of Russian Academy of Sciences, Academic Vonsovsky str., 15, 620016 Ekaterinburg, Russia

[2] Institute of Mineralogy South Urals Research Center of Mineralogy and Geoecology of the Urals Branch of the Russian Academy of Sciences, Ilmeny Reserve, 456317 Miass, Russia; maslennikov@mineralogy.ru (V.V.M.); artemyev@mineralogy.ru (D.A.A.); celyukoa@rambler.ru (A.S.T.)

[3] Geological Department, South Ural State University, Lenin av., 76, 454080 Chelyabinsk, Russia

* Correspondence: ivanovks55@ya.ru

Received: 26 February 2020; Accepted: 15 May 2020; Published: 17 May 2020

Abstract: In the Bazhenov Formation, framboidal clusters and nodular pyrite formed in the dysoxic–anoxic interface within organic-rich sediments. Some nodule-like pyritized bituminous layers and pyrite nodules are similar to pyritized microbial mat fragments by the typical fine laminated structure. Framboidal pyrite of the Bazhenov Formation is enriched in redox-sensitive elements such as Mo, V, Au, Cu, Pb, Ag, Ni, Se, and Zn in comparison with the host shales and nodular pyrite. Nodular pyrite has higher concentrations of As and Sb, only. Strong positive correlations that can be interpreted as nano-inclusions of organic matter (Mo, V, Au), sphalerite (Zn, Cd, Hg, Sn, In, Ga, Ge), galena (Pb, Bi, Sb, Te, Ag, Tl), chalcopyrite (Cu, Se) and tennantite (Cu, As, Sb, Bi, Te, Ag, Tl) and/or the substitution of Co, Ni, As and Sb into the pyrite. On the global scale, pyrite of the Bazhenov Formation is very similar to pyrite from highly metalliferous bituminous black shales, associated, as a rule, with gas and oil-and-gas deposits. Enrichment with Mo and lower Co and heavy metals indicate a higher influence of seawater during formation of pyrite from the Bazhenov Formation in comparison to different styles of ore deposits. Transitional elements such as Zn and Cu in pyrite of the Bazhenov Formation has resulted from either a unique combination of the erosion of Cu–Zn massive sulfide deposits of the Ural Mountains from one side and the simultaneous manifestation of organic-rich gas seep activity in the West Siberian Sea from another direction

Keywords: framboids; pyrite; trace elements; bituminous shale; metals; Bazhenov Formation

1. Introduction

In recent years, higher contents of chalcophile elements (Cu, Zn, As, Se) have been recognized in bituminous clayey–siliceous black shales of oil-bearing Bazhenov Formation (Late Jurassic period J_3). The average contents of specific trace elements in the black shales are as follows (ppm): Zn (988), Cu (199), As (67); Se (34.7), Cd (22.8), In (1.4) and are higher than worldwide values; other elements Pb (15.7), Ga (15), Sb (9.8), Ag (1.4), Hg (0.2) are around the level of worldwide values; and a third group, Tl (2.3), Ge (3.0), Bi (3.4) and Sn (4.0) are below worldwide values [1]. It has been hypothesized that the majority of chalcophile trace elements in these rocks formed under reducing conditions of slow sedimentation are captured from seawater by organic matter and, accordingly, by pyrite [1]. In oil-bearing and barren black shales, pyrite is one of the most important hosts of metals [2–5].

Very often, different styles of pyrite-rich high metalliferous black shales are associated with oil, gas and with massive sulfide deposits. Black shales and enclosing authigenic pyrite, associated with oil-and-gas and gas fields, are commonly highly metalliferous (average trace element contents (ppm):

Ni 1700, Zn 1400, Cu 860, Ag 180, V, Se 890, Mo 82, Cd 70) [6]. Recognition of the geochemical features of the metalliferous black shale varieties associated with a different style of deposits is an important step in elaboration of prospection criteria. Several hypotheses explain the metal concentration in black shales. The numerous genetic models are based on analysis of redox conditions and consequent metal concentration directly in euxinic seawater or in dysoxic–anoxic seawater/sediments interfaces]. These models are supported by direct observation and complex analyses of modern dysoxic, anoxic and euxinic basins. Pyrite can take up different assemblages of trace elements depending on whether it forms syndiagenetically (As, Mo, Sb) or diagenetically (Co, Cu, Ni, and Pb) [3,5,7–10]. In some research, weathering of continental crust, as well as active hydrothermal activity, are considered as a main processes of nutrient elements enrichment in the ocean [11].

In contrast, a petroleum-exhalative hypothesis has been developed to explain high concentrations of metal in black shales [12]. This model is based on analyses metal enrichment in hydrothermal petroleum in modern hydrothermal systems of sediment-covered spreading centers [13] and data on high solubility of the trace elements in petroleum [12]. Hydrothermal activity is sometimes considered as helpful for the increase of reducibility of seawater and enhancing shale gas [14].

Sedimentary-diagenetic pyrite is a stable mineral, which preserves the entire spectrum of trace elements and their contents up to temperatures of the greenschist facies metamorphism [15]. Transformations of host rocks of the oil-bearing Bazhenov Formation [16] barely reached the stage of mesocatagenesis and, therefore, they should be considered as a most suitable mineral for studying the chemistry of authigenic pyrite. The Bazhenov Formation hosts a huge volume of pyrite-rich black shales where pyrite yields high redox-sensitive metal potential. However, the concentration of trace elements in pyrite of the Bazhenov Formation before have not been determined. Rocks, which were subject to hydrothermal alteration, are not discussed in the present paper.

In recent years, the study of trace elements in pyrite has become possible at a new level owing to implementation of a revolutionary new method of high-resolution microanalysis of minerals—laser ablation-inductively coupled plasma-mass spectrometry (LA–ICP–MS) [17]. As a rule, the main concentrators of chalcophile elements and gold in black shale sequences, including gold-bearing, oil-bearing, pyrite-bearing and barren ones, are framboidal pyrite and, to a lesser extent, pyrite nodules [11,15,18,19]. These varieties of pyrite are widespread in black shales of the Bazhenov Formation.

In connection with the aforementioned, the purpose of the present paper is to show the highly metalliferous potential of authigenic pyrite from the black shales of the Bazhenov Formation. The other objective is the determination of trace element forms and mineral chemical assemblages in framboidal and nodular pyrite varieties. The geochemical comparison of pyrite in the Bazhenov Formation with pyrite from ore deposits generally is also included in the paper. We also discuss possible causes of trace element concentration in the pyrite varieties.

2. Methods

LA–ICP–MS was applied to determine trace elements. The LA-ICP-MS methodology is described in detail in [15,17]. An Agilent 7700x quadrupole mass spectrometer with a New Wave Research UP-213 laser ablation system were used for research (the Institute of Mineralogy SU FRC MG UB RAS, Miass, Russia). The data obtained were processed with Agilent MassHunter Workstation Software (version 4.3). Check analyses were performed at the Centre for Ore Deposit and Earth Sciences (CODES) (University of Tasmania, Hobart, Australia).

The Nd:YAG laser settings: wavelength—213 nm, fluence—2.5–3.5 J/cm^2, pulse repetition rate—7 Hz, spot diameter 25–40 μm, in special cases 10 μm (pyrite framboids). Carrier gas—He, gas flow rate—0.6 L/min. Laser operation time: 5 s (pre-ablation) and 30 s (blank analysis); the ablation time—35–50 s. The time between pre-ablation and ablation—15–25 s. Mass spectrometer settings were as follows: RF power—1450 W, carrier gas—Ar, carrier gas flow rate—0.95 L/min, plasma support gas flow—15 L/min, cooling gas flow—0.9 L/min. The mass spectrometer was calibrated with NIST SRM-612 glass. Production of molecular oxide species (i.e., $^{232}Th^{16}O/^{232}Th$) was maintained at levels below 0.3%.

The contents of 21 trace elements were determined in sulfides: ^{51}V, ^{53}Cr, ^{55}Mn, ^{57}Fe, ^{59}Co, ^{60}Ni, ^{65}Cu, ^{66}Zn, ^{75}As, ^{77}Se, ^{95}Mo, ^{107}Ag, ^{111}Cd, ^{118}Sn, ^{121}Sb, ^{125}Te, ^{182}W, ^{197}Au, ^{205}Tl, ^{208}Pb, and ^{209}Bi. Integration time—10 ms (excluding Ni, Ga, Ge, Se, Te—20 ms; Ag, Au—30 ms). The standard values are not certified and should be used with caution: ^{72}Ge, ^{77}Se, ^{115}In, ^{125}Te, ^{197}Au, ^{205}Tl, and ^{209}Bi. Due to polyatomic interferences with ^{40}Ar + ^{32}S and ^{56}Fe + ^{16}O, ^{72}Ge values are conditional.

For calibration and calculation, the international standard of pressed sulfide USGS MASS-1 has been used [20]. The calibration standard was analyzed every 10–13 spots to account for the instrument drift. The calculation was performed using the Iolite software (version 2.5) [21] using ^{57}Fe as internal standard. The sum of cations together with Fe was equal to 46.5%.

The LA-ICP-MS data were processed in the Statistica program v.10 using correlation analysis. The trace element associations have been calculated by the method of "maximal correlation way" (MCW) [22]. The source material is half the square correlation matrix, in which only statistically significant correlation coefficients are recorded. The maximum modulus of the correlation coefficients are ranged for each following element. New selections were not made if the element with maximum correlation coefficients has already been selected. Several highs (association) are divided by minimum values of the correlation coefficients.

3. Geological Position and Composition of the Host Rocks

The Bazhenov Formation is distributed throughout the West Siberian Plate covering an area of more than 1 million km^2 [23] (Figure 1). The Bazhenov Formation includes the Late Jurassic pyrite-bearing black shales, represented by bituminous varieties [7,24]. Bituminous shales studied in several areas contain mostly pyrite nodules and framboidal pyrite. In this paper, we compile data from many drill cores with study of numerous polish thin sections and samples for mineralogical research from different pyrite occurrences of Bazhenov Formation [24]. From 4 drill cores we choose 5 pyrite-rich samples which we considered to be the best for LA-ICP-MS analyses and genetic interpretation (Table 1).

Table 1. The host rocks of the studied Bazhenov Formation sections.

Sample No.	Area	Borehole	Depth, m	Rock
sal-2802-1002	Salym	2802	2792.5	Bituminous black shale enriched with pyrite, carbonate and barite
kog-163-1499	Kogalym	163	2889.5	Bituminous black shale with glauconite
liv-131-1540	Livadiya	131	2746.5	Bituminous black shale
liv-131-1532	Livadiya	131	2742.5	Bituminous black shale with radiolarian shells
vat-1190-864	Vat'egan	1190	2833.5	Bituminous silica-rich black shales with remains of radiolarian shells, replaced by pyrite

Bituminous or carbonaceous black shales are dark brown rocks with thinly laminated texture, containing ultrafine-grained quartz (up to 50–85%), fragments of K feldspar and quartz (2–3%). In some rock varieties, calcite, dolomite, and barite are common. Hydromica (5–25%), illite–smectite (1–10%), and kaolinite (2–5%) predominate among layered silicates. Among other minerals from bituminous deposits of the Bazhenov Formation are pyrite, sphalerite, marcasite, barite and apatite [24].

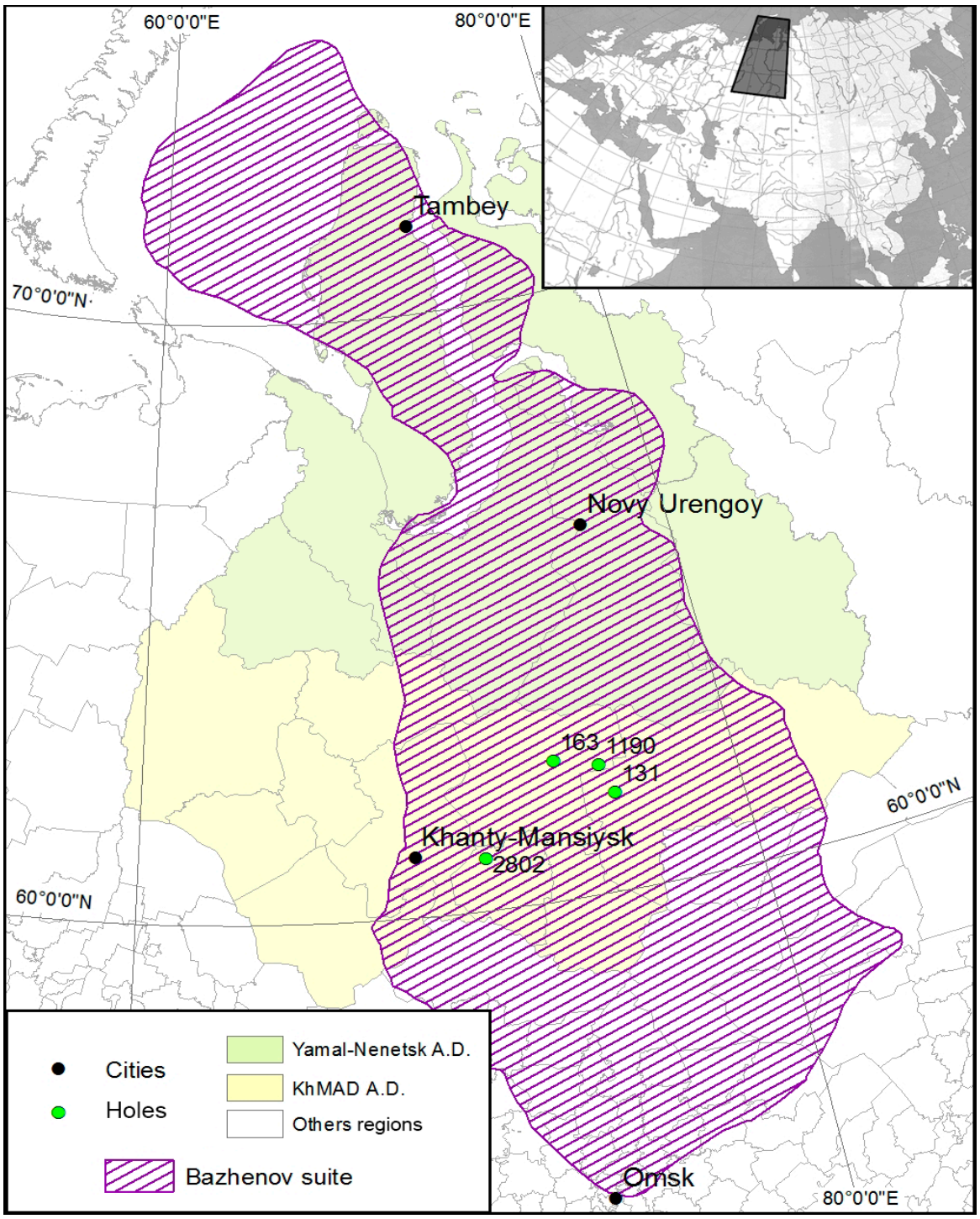

Figure 1. Map of Bazhenov Formation sediments on the West Siberian plate in Russian Federation. A.D.—autonomous district.

An interval of radiolarian assemblages in the Bazhenov deposits contain interbeds and lenses with abundant pyrite nodules. A characteristic feature of the bituminous shales is the presence of diverse morphogenetic varieties of pyrite. Pyrite occurs as small lenses, microtubules, rounded micronodules, and finely dispersed inclusions [25]. Framboidal pyrite and crystalline pyrite nodules predominate in our samples. The former occurs as single globules, which are disseminated in the matrix of black shales are often invisible against the background of larger nodule-like pyritized bituminous layers (Figure 2a). It is inferred that this type of pyrite nodule developed along the bedding (see Figure 2a), which has inherited the thinly laminated structure of microbial mats. They contain inclusions of pyritized radiolarians and interbeds of the organic-poor matrix. Pyrite

framboids are much less common in the form of clusters or nodules, applicable to LA-ICP-MS analysis (Figure 2b). The maximum measured size of a single framboid is 32 μm. Sometimes, framboids fill cavities of pyritized microfossils (Figure 2c). The fine-grained pyrite nodules are transformed sporadically into coarse-grained pyrite–marcasite aggregates (Figure 2d). The typical laminar mat-related structure is retained in the fine-grained part of these pyrite nodules (Figure 2e). Similar laminated nodule-like microbial mat structures are recognized in other black shale occurrences of a wide range of ages and geography [26]. Barite is common in bituminous shales. Visible chalcopyrite accumulations occur only in altered bituminous carbonate-bearing shales in association with pseudomorphic pyrrhotite and chalcopyrite, developed after framboidal pyrite. (Figure 2f) The framboidal and nodular pyrite without visible micro-inclusions are the focus of this research.

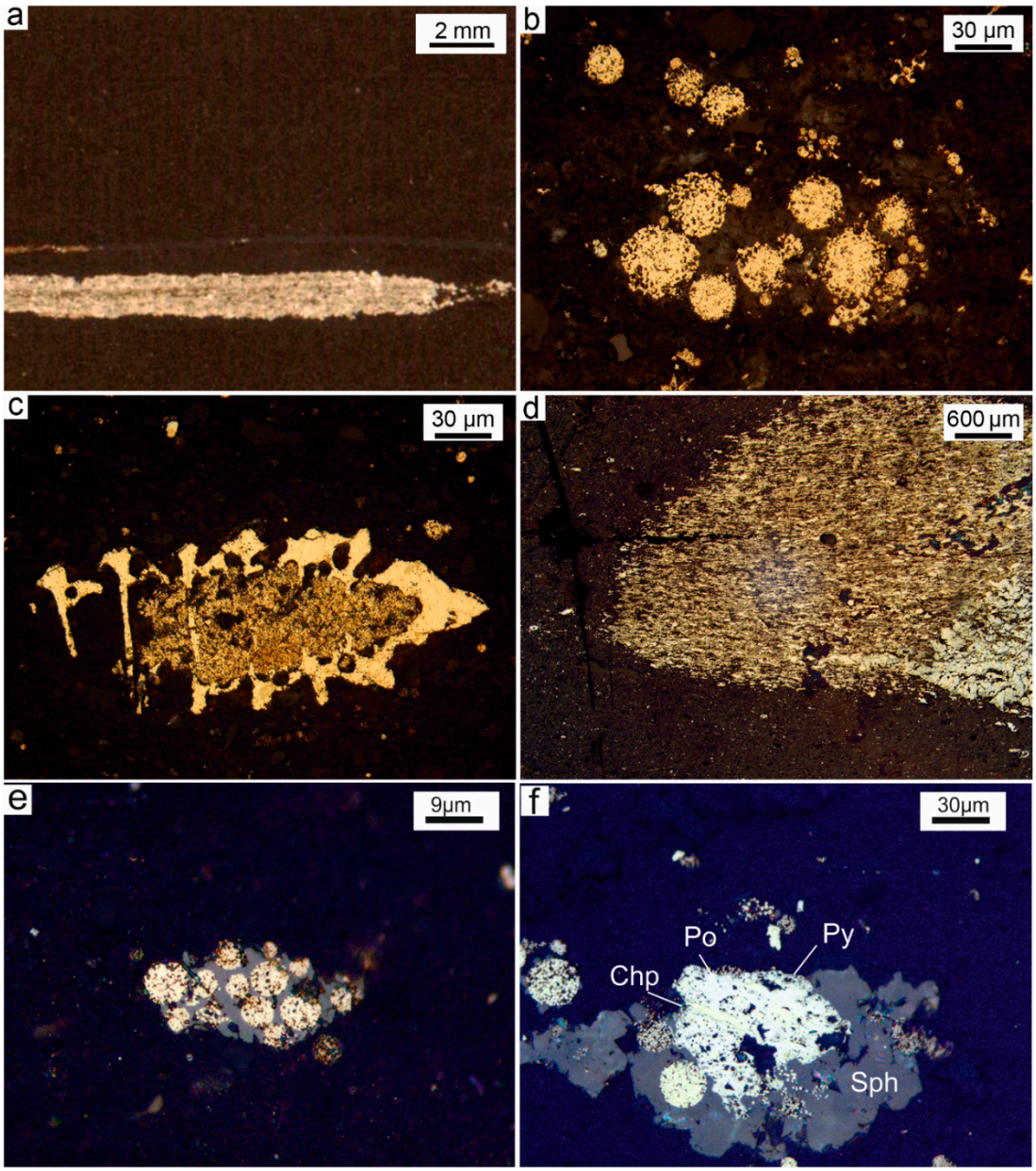

Figure 2. Pyrite varieties from black shales of the Bazhenov Formation. (**a**) pyritized nodule-like bituminous layers in in black shales; (**b**) framboidal pyrite in carbonaceous shale; (**c**) framboidal pyrite in a cavity of radiolarian pyrite pseudomorph; (**d**) nodule-like pyrite with laminated mat-related structure in black shale; (**e**) framboidal pyrite cluster cemented by sphalerite; (**f**) micro-inclusions of framboidal and fine-grained pyrite (Py) by chalcopyrite (Chp) and pyrrhotite (Po) in sphalerite (Sph) aggregate. Reflected light.

4. Trace Elements of Pyrite Varieties

Framboidal and nodular varieties of pyrite are essentially different from each other and from the host rocks in terms of a spectrum and contents of chemical elements.

Zinc (Zn). Framboidal pyrite from deposits of the Bazhenov Formation is characterized by abnormally high Zn content (up to 8.8 wt. %) This anomalously elevated content point to nano-inclusions of sphalerite in framboidal pyrite. Because the maximum Zn contents are commercially important, it is the dominant element in a spectrum of other related elements. The average Zn content in framboidal pyrite from shale of the Bazhenov Formation is higher (988 ppm) than other global metalliferous shales [1]. The Zn content in nodular pyrite is characterized by one to two orders of magnitude lower mean and median values (Table 2).

Table 2. Trace elements in framboidal pyrite from carbonaceous shales of the Bazhenov Formation, ppm.

Framboidal Pyrite													
Elements	**NAS**	**V**	**Cr**	**Mn**	**Co**	**Ni**	**Cu**	**Zn**	**As**	**Se**	**Mo**	**Ag**	**Cd**
av	39	155	607	1439	272	1138	2407	2839	361	184	487	15	67
std		213	1338	1238	170	469	2256	14,024	226	146	207	19	378
min		5.7	6.1	35	9.3	447	241	34	71	29	186	1.3	0.1
max		1010	7400	3870	599	2290	7080	88,000	804	455	1050	57	2360
med		111	200	723	262	1070	864	366	249	108	448	4.2	1.1
gm		54	183	945	198	1046	1398	468	293	130	448	7.0	1.5
Elements	**NAS**	**Sn**	**Sb**	**Te**	**W**	**Au**	**Hg**	**Tl**	**Pb**	**Bi**	**Ga**	**Ge**	**In**
av	39	1.4	66	0.8	0.3	0.5	2 0	18	252	36	93	41	0.08
std		3.0	58	0.8	0.3	0.2	5.2	12	298	4.2	49	13	0.358
min		0.1	9	0.0	0.0	0.1	0.1	4.3	16	0.2	0.01	0.2	0.001
max		19	178	2.8	1.0	1.2	33	69	926	14	307	83	2.250
med		0.7	29.8	0.3	0.1	0.6	0.9	16	52	1.0	0.5	1.6	0.009
gm		0.7	41.8	0.4	0.1	0.5	1.0	15	101	1.6	0.3	1.8	0.011
Nodular Pyrite													
Elements	**NAS**	**V**	**Cr**	**Mn**	**Co**	**Ni**	**Cu**	**Zn**	**As**	**Se**	**Mo**	**Ag**	**Cd**
av	62	19	26	91	12	64	54	69	1914	74	266	0.5	2.7
std		16	22	194	18	121	84	204	2221	121	259	1.1	4.9
min		0.4	0.7	0.6	0.08	0.8	0.7	1.0	6.2	2.9	1.4	0.02	0.01
max		61	118	1378	91	829	555	1280	7870	606	829	8.1	34
med		12	25	17	3.1	23	19	5.,5	449	28	151	0.2	1.2
gm		10	15	23	2.7	20	20	10	440	30	107	0.3	1.1
Elements	**NAS**	**Sn**	**Sb**	**Te**	**W**	**Au**	**Hg**	**Tl**	**Pb**	**Bi**	**Ga**	**Ge**	**In**
av	62	0.5	142	0.05	0.2	0.1	0.4	9.4	5.3	0.05	1.3	1.1	0.006
std		0.3	218	0.05	0.3	0.2	0.3	7.1	9.1	0.08	1.6	0.3	0.010
min		0.1	0.5	0.003	0.00	0.001	0.04	3.1	0.1	0.000	0.01	0.3	0.000
max		1.8	1063	0.20	1.1	0.7	1.2	37	53	0.51	8.5	2.2	0.055
med		0.4	35	0.03	0.10	0.03	0.3	7.3	2.1	0.01	0.5	1.1	0.003
gm		0.4	37	0.03	0.06	0.05	0.3	7.8	2.0	0.02	0.5	1.1	0.003

Note: NAS—number of analysis spot, av—average, std—standard deviation, min—minimum contents, max—maximum contents, med—median, gm—geometric mean.

The correlation analysis of the composition of bituminous sedimentary rocks has revealed a significant positive correlation of Zn with organic matter and high correlation with degree of pyritization against the background of a negative correlation with the clayey material [1]. In fact, there is a positive correlation between Zn and such organophile elements as V, Mo and Au. In the correlation series of mineralogical and geochemical associations Zn together with Cd ranks first (Table 3). Based on the results of the correlation analysis of the data on both pyrite varieties, Zn is correlated with elements (Cd, Sn, Hg, Ga, Ge, and In), which are common isomorphic admixtures in the sphalerite structure. This is also confirmed by the mineralogical data [24]: Zn occurs mainly as sphalerite micro-inclusions in framboidal pyrite. Zn carbonates and aluminosilicates have not yet been determined.

Table 3. Series of mineralogical-geochemical associations of morphogenetic pyrite varieties of the Bazhenov Formation.

Pyrite Varieties	Associations of Chemical Elements
Framboidal	I(Cd + Zn + Ga + Ge + In + Hg + Sn) + II(V + Mo + Tl + Au) + III(Co + Ni) + IV(Cu + Se + Sb + Mn) + Ag + V(As + Pb + Bi + Te) + W–Cr
Nodular granular	I (Cd + Zn + In) + II(Ga + V + Au + W + Sn) + III(Co + Ni + Pb + Ag) + IV(Se + Sb + As + Tl) + V(Cu + Mn + Bi) + VI(Hg + Mo)–Ge–Te–Cr

Cadmium (Cd). The Cd content in shales (22.8 ppm after [1]) of the Bazhenov Formation only slightly exceeds the average worldwide values in black shales (9 ppm after [27]). The median Cd contents in both pyrite varieties are extremely low, while in Zn-rich samples they reach 0.2 wt. % (see Table 2). The Cd distribution is non-uniform.

The correlation analysis of sedimentary rocks of the Bazhenov Formation has revealed a significant positive correlation between Cd with sulfide sulfur, organic carbon, degree of pyritization of iron and a significant negative correlation with the clay minerals. Cadmium in both varieties of pyrite shows positive correlation with elements, characteristic of sphalerite (Zn, Hg, Ga, In, Sn), as well as with typical organophilic elements such as V, Mo and Au [27].

Copper (Cu). Along with Zn, framboidal pyrite from the Bazhenov Formation contains a large amount of Cu (up to 0.7 wt. %). The Cu–Zn diagram shows the direct correlation of contents of these elements (Figure 3) that is evidence of thin intergrowths of sphalerite and Cu chalcogenides, for example, emulsion intergrowths of chalcopyrite or tennantite in sphalerite. The average Cu concentration in framboidal pyrite are one–three orders of magnitude higher (see Table 3), than those obtained for pyrite nodules (see Table 2) and for clayey–siliceous shales (199 ppm after [1]). The correlation analysis has revealed a significant positive correlation between Cu and organic carbon, sulfide sulfur, and degree of pyritization against the background of negative correlation with the clayey material [1]. However, as evidenced from the results of the correlation analysis, there is a negative correlation between Cu and typical organophilic elements, such as V and Mo.

Using the maximum correlation path method [22], it was found that Cu in framboidal pyrite forms a unified series with Sb, Se and Pb (IV in Table 3). The Cu–Sb association is evidence, at the least, of the presence of nano-inclusions of Cu–Pb sulfosalts or a galena–tennantite paragenesis. The copper in framboidal pyrite is correlated positively with elements, characteristic of tennantite (As, Sb, Ag, Se, Te, Bi) and galena (Pb, Bi, Ag, Sb). The possible occurrence of tennantite is confirmed by directly proportional dependence of Cu, As, and Sb contents in Cu–As, Cu–Sb and Sb–As diagrams (see Figure 3). The correlation of Cu with Mn is enigmatic for interpretation.

Correlation coefficients, calculated for nodule pyrite, are somewhat different: As and Sb have negative values, probably due to transformation of tennantite into chalcopyrite. The nodular pyrite is characterized by positive relationships of Cu with such organophilic elements as V, Mo and Au, as well as with Hg, Tl, and Ga.

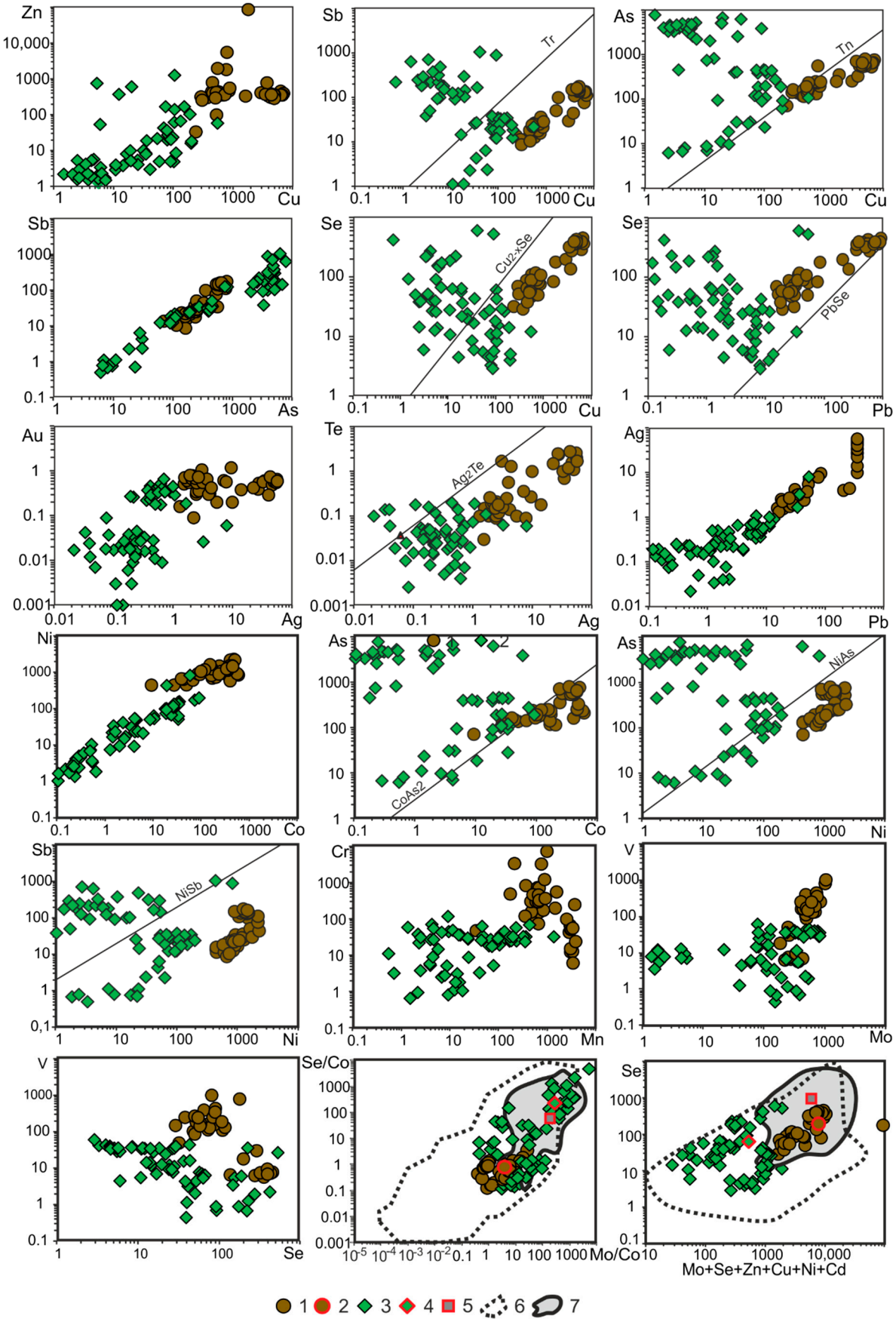

Figure 3. Distribution diagrams of trace element contents in framboidal (1) and nodular (3) varieties of pyrite from the Bazhenov Formation. (2, 4) average contents; (5) average contents in sedimentary–diagenetic pyrite according to [19]; (6) fields of pyrite from black shales, (7) fields of pyrite from high-metal black shales.

Lead (Pb). The Pb content in framboidal pyrite from the Bazhenov Formation deposits is one-two orders of magnitude higher than that in pyrite nodules (see Table 2) and host bituminous clayey–siliceous shales (15.7 ppm after [1]). The maximum Pb contents reach 0.09 wt. %. It was established that Pb was not accumulated in association with organic matter in the Bazhenov deposits [28,29]. This conclusion was confirmed by Zanin et al. [1] based on the correlation analysis results, which showed a significant positive correlation between Pb and the clayey material at a significant negative correlation with sulfide sulfur, organic carbon and degree of pyritization.

However, the correlation analysis of framboidal pyrite has revealed not only higher Pb content than that in the host rocks, but also the close relationships between Pb and Bi, Ag, Te, Sb, and Se, which are typical isomorphic admixtures in galena, and with elements of copper sulfosalts (Cu, As, Sb, Te, Bi, Se), close to tennantite (see Tables 3, S1 and S2).

In Pb–Se diagram, the line, corresponding to clausthalite, outlines the field of pyrite measurement points from higher Pb contents, than is typical of clausthalite. However, the Pb contents are not so high that clausthalite or galena were easily detected. The Pb contents in framboidal pyrite are only an order of magnitude higher than that in mudstones of the Bazhenov Formation as a whole [1]. In turn, the Pb content in nodular pyrite in only half of all cases is slightly lower than that in framboidal pyrite (Table 2, Figure 3).

Mercury (Hg). The Hg content in deposits of the Bazhenov Formation ranks very low; none of the samples reaching 1 ppm [1]. At low average Hg content, the maximum values (up to 33 ppm) were detected when analyzing Zn-rich framboidal pyrite. The correlation analysis has revealed the close relationships of Hg with elements, characteristic of sphalerite (Zn, Cd, Sn, Ga, Ge, In) (see. Table S1). At the same time, a positive correlation with such organophilic elements as V, Mo, and Au was established. In nodular pyrite, there is no correlation with Zn, but there is a positive correlation between Hg and Mn, Co, Ni, and Cu and a negative correlation with As and Sb. The latter indicates the appearance of chalcopyrite nano-inclusions in pyrite nodules.

Selenium (Se). On average, the Se content in framboidal pyrite is 5–6 times more (see Table 2), than that in host black shales (34.7 ppm after [1]). The average Se content in nodular pyrite is only two times higher than that in host rocks, while maximum contents are higher than those in framboidal pyrite. The correlation analysis of bituminous deposits of the Bazhenov Formation has revealed a significant positive correlation between Se and sulfide sulfur, organic carbon, degree of pyritization and a significant negative correlation with the amount of the clay minerals [1]. However, in both pyrite varieties, a negative correlation between Se and V does not confirm the relationship of Se with organic matter (See Table 3). On the contrary, Se is correlated with Mn. A negative correlation between Se and Mo in framboidal pyrite is of specific interest that contradicts modern models of the joint accumulation of these elements [11].

In general, the Se content is correlated with a wide spectrum of chemical elements, including those in pyrite (Co, Ni), nano-inclusions of galena (Pb, Se, Bi, Sb, Ag, Tl, Te), chalcopyrite and tennantite (Cu, As, Sb, Tl, Se, Te) associations. It is of interest that the correlation between Se and Co disappears in nodular pyrite. There is a significant negative correlation of Se with Ga.

In the Cu–Se diagram, the field of measurement points of framboidal pyrite is shifted from the $Cu_{2-x}Se$ line towards the predominance of Cu that is characteristic of chalcopyrite and tennantite nano-inclusions. A significant part of measurement points of nodular pyrite is shifted towards the Se field. It is likely that, in this case, a larger amount of Se enters the structure of granular nodular pyrite than the structure of the framboidal variety. This is also observed in the Pb–Se diagram, where Se/Pb ratio is equal to or greater than in clausthalite. It is known that incorporation of Se into the structure of pyrite is supported by high temperatures of mineral genesis [30]. In addition to temperature, the higher Se contents may reflect the strong pH-Eh dependence of the dissociation constant for H_2Se [31]. Se exist as S (IV) or S (VI) in oxic seawater and as elemental Se or reduced selenide Se^{2-} in anoxic waters [32]. Selenate and selenite are highly soluble and mobile in contrast to elemental Se and selenides [33]. A potential sink of Se in marine sediments may be pyrite, which can catalyze Se reduction to selenide and incorporates Se in suboxic sediments [34].

Tellurium (Te). The Te content in bituminous rocks of the Bazhenov Formation is rarely over 1 ppm [1]. Only in a single case, the maximum Te content in framboidal pyrite reaches 2.8 ppm. The Te content in framboidal pyrite shows a significant negative correlation with such organophilic elements as V and Mo. Significant positive correlation relationships between Te and elements, characteristic of tennantite (Cu, As, Sb, Ag, Se), galena (Pb, Tl, Sb, Ag, Se) and pyrite (Co, Ni, Mn) were revealed (see Tables S1). However, almost all of these elements can enter into the structure of pyrite in the form of an isomorphic impurity. In nodular pyrite, all these bonds disappear when a positive correlation with Sn and Au appears.

Arsenic (As). The average As content in framboidal pyrite (see Table 2) is five times higher than that in host black shales of the Bazhenov Formation (67.4 ppm after [1]). However, the average As content in nodular-like pyrite is even much higher (0.2 wt. %) at the maximum content of 0.8 wt. %. The correlation analysis of the composition of host rocks has revealed a significant positive correlation between As and sulfide sulfur, organic matter, and degree of pyritization of iron against the background of a significant negative correlation with the clayey material [1]. However, there is no correlation between As and V or Mo in framboidal pyrite, while in the case of nodular pyrite, the correlation is negative.

The positive correlation between As and Sb in nodular pyrite is clearly evident in the As–Sb diagram (see Figure 3). The Cu–As diagram shows that measurement points are close to the tennantite line ($Tn_{90}Tr_{10}$) (see Figure 3). However, the field of measurement points with higher As contents is outlined in the same diagram. It is believed that As in black shales is associated usually with pyrite [35]. Very low dissolved As concentration may influence Cu behavior in sulfidic sediments, where dissolved Cu–As–S complexes determine the bioavailability and mobility of Cu [36]. A positive correlation of As with Co, Ni and Mn, calculated for framboidal pyrite (see Table S1), shows that at least a small proportion of As occurs in the composition of pyrite as substitution in the lattice. However, such a correlation is absent in the matrix, calculated for nodular pyrite (see Table S2).

Antimony (Sb). The average Sb content in host black shales of the Bazhenov Formation is 9.8 ppm after [1] that is close to the average worldwide value in black shales (8.8 ppm after [27]). The average Sb contents in both pyrite varieties are 5–15 times higher than the average worldwide value (see Table 2). The maximum Sb contents (up to 0.1 wt. %) were determined in nodular pyrite. Based on the data of correlation analysis of the composition of deposits of the Bazhenov Formation, the Sb content shows a significant positive correlation with sulfide sulfur, organic carbon, degree of pyritization, as well as a significant negative one with the clayey material [1]. The correlation analysis of both pyrite varieties has revealed the most significant correlation between Sb and a complex of following trace element—Cu, Ag, As, Se, Pb, Bi, Te, which, most likely, corresponds to the galena–tennantite paragenesis. A correlation between Sb and organophilic elements (V, Mn) is negative or absent. The nodular pyrite shows a positive correlation of Sb with Au and W.

A correlation between Sb and Co, Ni in framboidal pyrite is insignificant, while that in nodular pyrite is noted only for Ni. It is possible that a proportion of Sb can be incorporated isomorphically into not only the structure of tennantite and galena, but also into the pyrite structure as well as As.

Bismuth (Bi). The accumulation of Bi in framboidal pyrite is slightly more intensive than in nodular pyrite (see Table. 2) and host rocks (3.4 ppm after [1]). The correlation analysis has not revealed a correlation link between Bi and any other element in rocks [1]. The correlation analysis of framboidal pyrite has revealed various relationships between Bi and elements, typical of galena (Pb, Sb, Ag, Se), sulfosalts (Cu, As, Sb, Se) and, properly, fine-grained pyrite (Co, Ni). A correlation between Bi and V is negative, while between Bi and Mn it is positive. The correlation matrix of nodular pyrite shows relationships between Bi and V, Au, W, Ga, and Hg; there is no correlation between Bi and Ni, while the correlation with As and Sb is negative, while maintaining the close relationships with Cu and Pb, as well as with other aforementioned elements.

Thallium (Tl). The Tl content in framboidal pyrite (see Table 2) is an order of magnitude higher than that in bituminous clayey–siliceous shales of the Bazhenov Formation (see [1]). The correlation analysis of the Bazhenov bituminous deposits has revealed an insignificant positive correlation

between Tl and sulfur and/or with organic matter and an insignificant negative correlation with the amount of clay minerals [1]. The calculations, made for framboidal pyrite, have shown positive relationships between Tl and organophilic elements such as V, Mo, Au, as well as non-interpreted relationships with Co and W. These relationships are not observed in nodular pyrite, but there appears a significant positive correlation not only with Co, but also with Ni, Cu, As, Sb, Se, Pb and Ag. These relationships suggest the galena–fahlore paragenesis in association with crystalline-granular pyrite. It is known that Tl can be incorporated isomorphically in both pyrite and in fahlore and galena.

Gold (Au). In terms of the metalliferous potential of pyrite varieties, Au is of interest. The Au content in framboidal pyrite reaches 1.2 ppm, while median values are by almost two orders of magnitude higher, and then average values in siliceous black shales (8.5 ppb after [27]). It should be noted that the Au content of 0.1 ppm in framboidal pyrite from the black shale association should be considered as high or boundary when assessing the gold potential of black shale sequences [18].

As seen in the general Ag–Au diagram, constructed for framboidal and nodular pyrite varieties, a directly proportional correlation between these elements is observed, although it is not evident for each pyrite variety separately. The highest Au content is characteristic of framboidal pyrite (0.1–1.2 ppm), while that in some pyrite nodules is also increased (0.1–0.7 ppm). Along with organophilic elements, such as V and Mo, a correlation between Au and other elements is observed. Framboidal pyrite shows the stable positive correlation between Au and elements of the sphalerite association (Zn, Cd, Sn, Hg, Ga, In). A correlation between Au and Tl was revealed only for framboidal pyrite. In general, a correlation between Au and As, characteristic of gold-bearing pyrite is absent or negative (see Apps. I and II). In this case, probably, the incorporation of Tl into the crystal structure contributes to the gold accumulation in pyrite.

Silver (Ag). The Ag content in framboidal pyrite is approximately an order of magnitude higher than that in nodular pyrite (see Table 2) and in deposits of the Bazhenov Formation (1.4 ppm after [1]). In most cases, Ag prevails over Au (see Figure 3). The occurrence of Ag as a biogenic element [37], as well as Au [38], in framboidal pyrite can be associated with organic matter. Based on the correlation data, the Ag content has a positive correlation with sulfide sulfur, organic matter, and degree of pyritization, as well as a significant negative one with the clayey material [1].

However, according to the results of the correlation analysis of framboidal pyrite, the pattern is controversial. There is a significant inverse relationship between Ag and V and hence with organic matter. Silver can be equally ascribed to two geochemical associations: (Cu + Se + Sb + Mn) and (As + Pb + Bi + Te), which, in terms of contents of these elements, most likely belong to the tennantite–galena paragenesis with corresponding isomorphic admixtures in tennantite (Ag, Se, Sb, As, Bi, Te) and galena (Ag, Bi, Sb, Te, Se).

It is most likely that the correlation with Mn indicates initial joint precipitation of Ag with Mn hydroxides under alkaline oxidizing conditions, characteristic of seawater. Such boundary conditions, close to Eh = 0, are typical of formation conditions of framboidal pyrite, which develops after iron monosulfides [39]. In addition, the relationship of Ag with Ni and Co is observed in the correlation matrix of nodular pyrite that is evidence that Ag can be incorporated into the crystal structure of pyrite, as noted by many researchers. The disappearance of a significant positive correlation between Ag and Mn argues for the reducing formation conditions of pyrite nodules.

Nickel (Ni). The higher amount of Ni is partitioned between organic matter and pyrite [11]. In comparison with nodular pyrite, the metalliferous potential of framboidal pyrite is characterized by high Co and Ni contents—elements, which form the unified mineralogical and geochemical association (see Table 2). Nickel prevails over Co (Co/Ni < 1–0.1), that is typical of sedimentary pyrite; these two elements can be incorporated isomorphically into the structure of pyrite [11]. The concentration of As in pyrite also plays a role in the Co/Ni ratio (see Figure 3). In addition, nickel as a biogenic element, which commonly occurs in organic matter. The presence of nano-inclusions of stibnites is rather less likely.

Vanadium (V). Vanadium in framboidal pyrite occurs in significant amount, reaching 0.1 wt. %. (see Table 3, Figure 3). Vanadium is organophilic element under the surface conditions; it enters the

composition of oil, bitumens, and forms metal–organic complexes. The V content in framboidal pyrite is the same, as in oil and bitumens [40]. The V content in nodular pyrite is much less.

The strongest correlation of V is with Mo and Au most probably related to organic matter. There is significant inverse relationship between V and elements, corresponding to nano-inclusions of tennantite (Cu, As, Sb) and galena (Se, Ag, Pb, Bi). In nodular pyrite, on the contrary, there is a directly proportional relationship between V content and all of these elements, as well as with Co and Ni (See Tables S1 and S2). The relationship between V and Co, Ni, and Mo is typical of oils [40].

In the correlation series, calculated with the maximum correlation path method for framboidal pyrite, the association of V with Mo, Tl, and Au is clear. The same calculation, performed for nodular pyrite, provides the association of V with Ga, Au, W, and Sn. The stable relationship between V with Au may suggest that Au was extracted from seawater by V-bearing bitumen and then was concentrated in framboidal pyrite during the process of transition of iron monosulfides to disulfides [38]. This is also confirmed by high maximum Se contents, which is an indicator of increased oxygen content in the atmosphere [18]. The V–Se diagram shows an inversely proportional relationship in the distribution of these elements in both varieties of pyrite (see Figure 3).

Molybdenum (Mo). The Mo content in framboidal pyrite occurs in significant amounts, reaching 0.1 wt. %. Framboidal pyrite, as well as a part of nodular pyrite are enriched with this hydrogenic element, characteristic of the Phanerozoic seawater. It is likely that the incorporation of Mo into framboidal pyrite occurred due to sorption processes under the conditions of organic matter oxidation [38]. Another point of view is that the molybdate ion is converted into reactive thiomolybdate species and is subsequently incorporated into sulfides or scavenged by S-rich organic matter in sulfidic conditions of sediment pore waters or in water column [3,5]. Minimal deposition of Mo in organic-rich shales have been attributed to primary low SO_4^{2-} (i.e., [8]). Particle-reactive thiomolibdate in the presence of sufficient H_2S can lead to Mo uptake by Fe-sulfides [39,41].

Tungsten (W). The average W content in both pyrite varieties are low (0.2–0.1 ppm) at maximum values of 1.2 ppm. The correlation analysis of the composition of framboidal pyrite has revealed associations, characteristic of tennantite (Cu, As, Sb, Se, Ag), galena (Pb, Sb, Ag, Tl, Te), pyrite (Co, As, Se), as well as Mn. In the correlation matrix (see Apps. 1,2), calculated for nodular pyrite, the positive relationships of W with V, Mo, Au, and Hg and negative ones with As, Sb, and Se are observed. Rutile, captured from the matrix during the growth of pyrite crystals could be a principal source of W. For example, this process took place in black shales of the Kumtor gold-ore deposit [42].

Manganese (Mn). The Mn content in framboidal pyrite is high (see Table 2) and an order of magnitude higher than in nodular pyrite. This is in agreement with previously obtained data on the typochemistry of these pyrite varieties: for example, in black shale deposits of pyrite and gold-ore deposits [42–44]. Manganese can be incorporated into the structure of pyrite, while it is more likely that Mn can occupy vacant positions. Moreover, Mn can be partly associated with the lithogenic and carbonate component of shales.

Chromium (Cr). The maximum Cr concentration is characteristic of framboidal pyrite (0.7 wt. %), while maximum Cr contents in nodular pyrite is an order of magnitude lower (~0.1 wt. %). The content in black shales is known to be ~100 ppm [27]. Unlike many other elements, Cr in framboidal pyrite shows only a positive correlation with Ni and a weaker correlation with Bi. At this, the Cr content in nodular pyrite shows only an inversely proportional relationship between Se, As, and Sb (see Apps. I and II). In all cases, Cr occurs at the end of the correlation series (see Table 3).

Chromium is a biogenic element [37] and, therefore, should reflect to some extent an amount of organic matter and has a directly proportional relationship with V. However, this is not observed in our data. The biological significance of Cr is not well understood. One cannot rule out that the Cr occurrence is as an isomorphic element in hydromica and chrome spinel, which could be contaminated by a laser beam at the sampling of small pyrite framboids and thinly laminated nodular pyrite, enriched with relic layered aluminosilicate and detrital accessory minerals.

Tin (Sn). The Sn content in both pyrite varieties is low, reaching the maximum values up to 19 ppm in framboidal Zn-bearing pyrite (see Table 2). An average Sn content in pyrite (see Table 2) is approximately similar to that in black shales of the Bazhenov Formation: 0.77 ppm [1]. The correlation

analysis of bituminous sedimentary rocks of the Bazhenov Formation has revealed previously a directly proportional relationship between Sn content and the organic matter content and an inverse one between amounts of pyrite and organic matter [1]. The study of framboidal pyrite has revealed a directly proportional relationship between Sn and isomorphic elements in sphalerite (Zn, Cd, Hg, Ga, Ge, In), as well as organophilic elements such as V, Mo, Au (see Tables 2 and S1). In turn, these relationships are almost completely preserved in nodular pyrite (see Tables 2 and S2); positive relationships between Sn and Co, Ni, Cu, Mn, and W (see Tables 2 and S2) and negative relationships with As and Sb.

Gallium (Ga). In general, the Ga contents in framboidal and nodular pyrites is an order of magnitude lower than the world average contents in black shales (14–20 ppm after [27]) and bituminous deposits of the Bazhenov Formation (15–27 ppm after [1]) (see Table 2). It was previously established that Ga shows a significant positive correlation with the amount of clay minerals and a significant negative correlation with sulfur, organic carbon and degree of pyritization [1]. However, in our case, Ga in framboidal pyrite shows a positive correlation both with organophilic elements (V, Mo), and with elements of sphalerite isomorphic association (Zn, Cd, Sn, Hg, In, Ge).

In addition, nodular pyrite shows a direct proportional relationship of Ga with Cu and Co, and a negative relationship with As and Sb (see Tables S1 and S2). Both pyrite varieties are characterized by the presence of a stable Ga–Au association. It should be noted that Ga in other environments often demonstrates a dual character. In particular, Ga in ores of copper sulfide deposits is associated both with hydromica and chlorite, and with sphalerite [45]. The Ga content in some polymetallic ores reaches 400 ppm [40]. The decomposition products of aluminosilicates at the silicification of sediments during halmyrolysis could partially be a Ga source in sphalerite from the Bazhenov Formation. Halmyrolysis is the global process of silicification of volcanogenic and terrigenous deposits under slow sedimentation conditions [46].

Germanium (Ge). The Ge contents in framboidal and nodular varieties of pyrite (see Table 2) are lower than the world average values and are close to contents in black shales (0.9 ppm after [1]). The Ge content in framboidal pyrite is somewhat higher than that in nodular one, excluding single maximum Ge contents (up to 83 ppm) in analyses, which yielded high Zn contents. The previously performed correlation analysis of compositions of black shales has revealed a significant positive correlation of Ge with pyrite, organic matter, and degree of pyritization of sediments, as well as a significant negative one with the clayey material [1]. As for Ge, calculations performed for framboidal pyrite have revealed a positive correlation with both organophilic elements (V, Mo) and elements of the sphalerite isomorphic association (Zn, Cd, Sn, Hg, Ga, In). In nodular pyrite, these relationships are almost completely absent or are extremely weak (V, Sn, Co, In) (see Tables S1 and S2). Besides renierite, argyrodite, and germanite, the main Ge source in pyrite and stratiform Pb–Zn deposits is sphalerite [40]. Moreover, feldspars, rutile, magnetite, and organic matter, which were subject to halmyrolysis, could be sources of both Ge and Ga.

Indium (In). The In content is very often below the detection limits (about 0.1–0.01 ppm). However, contents of these chemical elements in Zn-rich framboidal pyrite (Zn 8.8 wt. %) become significant (see see Tables S1 and S2). Based on correlation relationships, Indium enters the structure of sphalerite.

5. Discussion

The framboidal pyrite and crystalline pyrite nodules are subdivided in Bazhenov Formation by microtextures and trace element concentration. The framboidal pyrite sizes vary from 8 to 32 μm and commonly form clusters. This suggests that the framboids have grown below the seafloor at the oxic-anoxic interface within sediments overlain by oxic water columns rather than in euxinic seawater columns. Framboids developed in euxinic conditions are generally small (up to 5 μm) with a narrow size range because the initial reaction rate is fast and pyrite formation occurs already within the water column [3,47–49]. There is no evidence of pyrite oxidation in seawater in our samples, except in the cases of abundant barite in black shales. Feldspar decay could be the main process of barite concentration in SO_4^{2-} enriched seawater. A high concentration of SO_4^{2-}, reoxidized from H_2S, on the

surface of decayed organic matter reacted with Ba^{2+} and then precipitated. The high content of $BaSO_4$ is therefore an indicator for high bioproductivity [50,51]. However formation of modern and Paleozoic stratiform barite at cold methane seeps on continental margins is considered, as well [52].

The variation from dysoxic to anoxic conditions could be considered as the best condition for pyrite formation and preservation in organic matter rich sediments in the Upper Jurassic period of the West Siberia Sea. This suggestion is confirmed by calculation of the index of syngenetic pyrite (ISPY), as a proportion of oxian-ionic and transition elements [4]:

$$ISPY = \Sigma O_{XAN}/(\Sigma_{OXAN} + \Sigma_{TM})$$

where:

$$\Sigma_{OXAN} = As + Mo + Se \text{ (ppm) in framboidal pyrite}$$

$$\Sigma_{TM} = Cu + Ni + Cu + Zn \text{ (ppm) in framboidal pyrite}$$

This index is used to evaluate a relative amount of syngenetic pyrite. The index should have low values for oxic–dysoxic environments and should be closed to 1 for euxinic environments with a high portion of syngenetic pyrite, but relatively high values are expected also for anoxic conditions with pyrite formed at the seawater/sediment interface [4]: The ISPY calculated for framboidal pyrite of the Bazhenov Formation displays average value 0.3 with standard deviation 0.14. This value is typical for framboidal pyrite formed in sediments below dysoxic to anoxic seawater. In pyrite of organic-rich mudstone formed in a normal oxygenated marine environment average ISPY is around 0.09 [4].

Some nodule-like pyritized bituminous layers and pyrite nodules with fine-grained laminated pyrite are similar by structure to pyritized microbial mat fragments [26]. Coarse-grained pyrite in the nodules results by crystallization from pore water undersaturated with respect to initial monosulfides toward the end of early diagenesis when pore water sulfide depleted or when the rate of sulfate reduction is low [53,54].

The geochemical variations are significant if we compare framboidal and nodular pyrite varieties, scattered in black shales of the Bazhenov Formation. In comparison with nodular pyrite, framboidal pyrite is characterized by the predominance of a wider spectrum of elements. The following series was calculated in descending order from average contents in framboidal pyrite normalized to those in nodular pyrite (ppm): Bi 68 → Pb 48 → Cu 45 → Zn 41 → Ag 29 → Cd 25 → Cr 23 → Co 22 → Ni 18 → Mn 16 → Te 15 → V 8 → Au 4 → Sn 2.8 → Se2.5 → Tl 1.9 → Mo 1.8 → W 1.2 → Sb 0.5 → As 0.2. Framboidal pyrite accumulates heavy metals, which enter the composition of sulfide geochemical association: Bi, Pb, Cu, Zn, Ag, Cd, Te, Au, and Co, as well as organophilic elements (Cr, V, Ni). It should be noted that some researchers refer to such elements as Cu, Zn, Cd, and Ag, contained in seawater, as biogenic [45]. Pyrite nodules, which were formed at the later diagenetic stage, accumulate only Sb and As.

Sometimes, the background sedimentary-diagenetic pyrite from black shale formations, which even show no connection with ore deposits, contain high concentrations of the majority of chemical elements [6]. At the global scale, pyrite from highly metalliferous bituminous deposits, associated, as a rule, with gas and oil-and-gas deposits, is characterized by higher Se content plus the complex of metals (Mo, Zn, Cu, Ni, Cd) [19]. The data of framboidal pyrite plotted on a Se–(Mo + Zn + Se + Cu + Ni + Cd) diagram lie in the field of pyrite from highly metalliferous black shales associated with oil-gas deposits (see Figure 3). In the Se/Co–Mo/Co diagram, most of the measurement points of the Bazhenov nodular pyrite occur in the field of pyrite from highly metalliferous deposits, while those of framboidal pyrite occupy the boundary zone between pyrites from highly metalliferous bituminous shales and from common background carbonaceous deposits (see Figure 3). In general, relationships between median trace element contents in studied framboidal pyrite from the Bazhenov Formation and those in sedimentary-diagenetic pyrite (framboids, small crystals) from world-wide black shales (after [19] form the following series in descending order (Bazhenov framboids/general framboids): Mo 22 → Au 18 → Zn 13 → Tl 4.4 → Cu 4.3 → Ni 2.7 → Co 2.6 → Ag 2.1 → Sb 1.3 → Te 0.5 → Pb 0.3. Thus, the occurrence of relative high Mo, Zn, and Au contents in framboidal pyrite of the Bazhenov Formation is clearly demonstrated. It is likely that thallium contributes to the

incorporation of Au into the Bazhenov framboidal pyrite lattice bound. In terms of the majority of trace elements, with the exception of Mo, the Bazhenov nodular pyrite compares significantly to the global background variety of sedimentary (sedimentary–diagenetic) pyrite (Bazhenov nodules/general sedimentary pyrite): Mo 7.5 → Tl 2.1 → Sb 1.5 → As 1.0 → Au 0.9 → Zn 0.2 → Ag 0.12 → Cu 0.10 → Te 0.07 → Ni 0.06 → Co 0.03 → Pb 0.001. The low contents of many elements are also connected with the high degree of crystallinity of most pyrite nodules from the Bazhenov Formation.

The comparison of framboidal and nodular varieties of pyrite from the Bazhenov Formation with pyrite from major ore-formational types of deposits provides interesting information about their metal bearing capacity. By now, the information on the median trace element contents was published without recognizing pyrite varieties in relation to different ore-formational types of deposits [19].

Framboidal pyrite from the Bazhenov Formation deposits is characterized by high contents of Mo, Tl, Sb, Zn, Cu and Ag in comparison with pyrite from gold–copper–iron skarn, porphyry copper–gold, and gold-ore orogenic deposits, being different from them in extremely low contents of Te and Co. The introduction of Te into ores of these deposits, as well as into ores of volcanogenic copper-zinc massive sulfide deposits, is associated with high-temperature slightly reduced hydrothermal fluids [55].

It should be noted that framboidal pyrite from the Bazhenov Formation is characterized by a high Au content compared to that from ore deposits generally, as well as to sedimentary pyrite from black-shale sequences which lack oil, gas and Pb–Zn massive sulfide deposits. In terms of Au concentration, framboidal pyrite from the Bazhenov Formation is close, on average, to that from copper sulfide deposits (Table 4).

Table 4. Median concentration of chemical elements in framboidal pyrite from the Bazhenov Formation are normalized to pyrite from major ore-formational types of deposits (Bazhenov framboids/ore-deposit pyrite).

Type of Deposit	Concentration Series											
Au–Cu–Fe skarn	Tl	Sb	Mo	Ag	As	Pb	Zn	Au	Cu	Ni	Te	Co
deposits:	4875	2986	1478	1434	966	300	242	153	110	0.8	0.5	0.005
Orogenic gold	Tl	Mo	Ag	Zn	Sb	Cu	Pb	As	Au	Te	Ni	Co
deposits	4875	2218	187	131	75	59	38	23	7.0	0.7	0.5	0.08
Porphyry copper	Tl	Sb	Pb	Ag	Mo	Cu	Zn	As	Au	Te	Ni	Co
deposits	4875	747	396	253	143	95	73	38	31	0.5	0.2	0.02
Pb–Zn black-shale	Au	Ag	Te	As	Tl	Sb	Mo	Zn	Cu	Pb	Ni	Co
deposits	77	3.9	3.0	2.7	2.4	2.1	2.0	1.5	0.8	0.5	0.13	0.10
Cu–Zn VHMS	Mo	Ni	Tl	Sb	As	Ag	Co	Au	Pb	Zn	Cu	Te
deposits	24	17	14	3.4	2.5	1.7	1.5	1.3	0.8	0.4	0.31	0.03

Note: VHMS—volcanogenic hydrothermal massive sulfide.

In comparison with pyrite from the major ore-formational types of deposits, nodular pyrite from deposits of the Bazhenov Formation contains higher contents of Mo, As, Sb, and Tl. According to [11,40], these elements are characterized by high contents in marine water (Table 5). Syngenetic pyrite formed within a euxinic water column is typically enriched in As, Mo and Sb but is low in heavy metals, and the geochemical variation reflects changes in seawater composition [3].

The only exception is abnormally high Tl contents in sedimentary–diagenetic pyrite from stratiform sulfide deposits of black-shale association, for which Tl is considered as a pathfinder indicator [56]. A significant number of other elements show minimum concentration coefficients (Co, Te, Pb). These are elements that occur in marine water in minimum concentrations [11,40].

The difference in concentration factors indicates the geochemical specialization of different ore-formational types of deposits. For example, pyrites from the copper–zinc massive sulfide deposits, which are associated with volcanogenic and sedimentary sequences, are characterized by higher median contents of the majority of trace elements (Zn, Cu, Mo, Pb, Tl, Sb) in comparison with pyrite from porphyry copper–gold, gold–copper–iron skarn and gold-ore orogenic deposits. The extremely low As concentration in pyrites are used to separate gold–copper–iron skarn (median value, 2.2 ppm)

and porphyry copper–gold deposits (53.4 ppm) [3]. Nodular-like pyrite is enriched in As in comparison to framboidal pyrite studied here. This may be caused by As-based metabolisms [57] in initial microbial mats or existence of marcasite enriched in As. The pyritized microbial mat structures are very well preserved in some pyrite nodules (see Figure 2d).

Table 5. Ranges of ratios of median contents of chemical elements, calculated for nodular pyrite from the Bazhenov Formation normalized to pyrite from major ore-formational types of ore deposits*.

Type of Deposit	Series of Relationships of Median Contents											
Au–Cu–Fe skarn deposits:	Mo	Sb	Tl	As	Zn	Ag	Cu	Au	Pb	Ni	Te	Co
	5018	875	726	179	11	8.2	6.7	2.8	1.7	0.4	0.022	0.002
Orogenic gold deposits	Mo	Tl	Sb	Zn	As	Cu	Ag	Ni	Pb	Au	Co	Te
	7528	726	22	6.0	4.2	3.6	1.1	0.2	0.2	0.13	0.03	0.03
Porphyry copper deposits	Tl	Mo	Sb	As	Cu	Zn	Pb	Ag	Au	Ni	Te	Co
	726	486	219	6.9	5.8	3.3	2.2	1.4	0.6	0.09	0.02	0.01
Pb–Zn black-shale deposits	Mo	Au	Sb	As	Tl	Te	Zn	Ni	Cu	Co	Ag	Pb
	6.7	1.4	0.6	0.5	0.4	0.13	0.07	0.06	0.05	0.04	0.02	0.003
Cu–Zn VHMS deposits	Mo	Ni	Tl	Sb	Co	As	Au	Cu	Zn	Ag	Pb	Te
	82	7.8	2.1	1.0	0.6	0.5	0.02	0.02	0.02	0.010	0.005	0.001

Note: data on ore deposits from [19].

The enrichment of Mo is known to occur in many Phanerozoic black shales, especially in those, which were formed under euxinic conditions [3]. It follows that Mo can be used to identify pyrite from the copper sulfide deposits of the sedimentary association (median value, 23 ppm), as well as background sedimentary–diagenetic pyrite (median value, 28 ppm). On the contrary, pyrite from volcanogenic copper sulfide deposits is characterized in most cases by low median Mo content (about 1 ppm). Pyrite from copper sulfide deposits is commonly enriched in Ag and Pb. This relates to both sedimentary deposits and volcanogenic deposits (median values: Ag 22 ppm and Pb 320 ppm). Pyrite from porphyry copper–gold deposits is Ni-rich (median value, 590 ppm) in comparison with other types of ore deposits. Pyrite from gold–copper–iron skarn formation is enriched in Co (median value, 1735 ppm). The mean Au content in pyrite from most of the studied deposits is close to the detection limits.

The enrichment of organic-rich mudstone with redox-sensitive and biophilic elements is usually connected with three main processes: (1) capture by phytoplankton and bacteria; (2) absorption on organic and detrital particles; (3) accumulation of Ni, Mo, Zn, As, Se, Cu, Pb and Sb in sedimentary–diagenetic pyrite during the diagenesis of iron monosulfides under oxidizing conditions [15,18].

Within the framework of development of a genetic model of the behavior of chemical elements under the formation of highly metalliferous pyrite varieties, it is necessary to consider possible sources of metals. The accumulation of abnormally high contents of metals in highly metalliferous bituminous deposits and, correspondingly, in pyrite has been under discussion for a long time [19]. Some researchers support a hydrothermal origin of metals, including their transfer from distal sources into seawater [58–60], while other researchers argue in favor of the model of transferring most metals to seawater under the weathering of the continental crust [39,61,62]. The consideration of Se or Se/Co, as indicators, recording degree of oxygenation of the atmosphere is of particular importance in the second model [11,63].

The oil deposits of the Bazhenov Formation are located above a rift system [64]. It could be inferred from this that the precipitation may be accompanied by hydrothermal activity similar to processes that formed framboidal and nodular pyrite in black shale hosted massive sulfide deposits. However, the direct comparison of these pyrite varieties with the similar types of framboidal and nodular pyrite of Safyanovskoe massive sulfide deposits [65]; display strong differences. The pyrite of the Bazhenov Formation contains relative higher Cr, V, Ni, Mo, which is related to an oceanic water source. In contrast, the same pyrite varieties located in the black shales of Safyanovskoe VHMS deposits are enriched with heavy metals (Bi, Pb, Ag, Au, Te) which are typical trace elements of massive sulfide ores. Concentration of transitional elements such as Zn and Cu in framboidal pyrite

are similar in both deposits (Table 6). However, the IXPY calculated for framboidal pyrite of Safyanovskoe deposit display very high average values (1.9) and standard deviation (2.1) in comparison to IXPY typical of pyrite from Bazhenov Formation (average value 0.3 with standard deviation 0.14). The cause is the highly variable composition of clastic sulfide turbidite transformed to framboidal pyrite layers resulting in different styles of diagenesis in the Safyanovskoe deposit [65,66]. Consequently, the framboidal pyrite formed in black shales of the Bazhenov Formation do not reflect a dramatic impact of typical hydrothermal massive sulfide fluids. The source of Zn and Cu in the Bazhenov Formation could be massive sulfide deposits of the Urals Mountains weathered at the same time rather than some hydrothermal source of these elements.

Table 6. Ranges of rations of median contents of chemical elements, calculated for framboidal (Py_f) and nodular (Py_{nd}) pyrite from the Bazhenov Formation (Bzh) normalized to the same pyrite varieties from the Safyanovskoe massive sulfide deposits (Saf).

Pyrite	Rations of Median Contents													
	Cr	**Co**	**V**	**Ni**	**Mo**	**Mn**	**Se**	**Zn**	**W**	**Cu**	**Tl**	**Sn**	**Cd**	**Au**
Py_fBzh/	125	19	15	5	4	3.9	3.0	1.0	0.6	0.6	0.5	0.5	0.4	0.21
Py_fSaf	**Sb**	**As**	**Te**	**Pb**	**Ag**	**Bi**								
	0.15	0.11	0.06	0.04	0.02	0.02								
	Cr	**V**	**Mo**	**Sn**	**Cd**	**W**	**Se**	**Ni**	**Co**	**Sb**	**As**	**Mn**	**Tl**	**Cu**
Py_{nd}Bzh	14	3.9	3.4	1.5	0.9	0.8	0.7	0.5	0.4	0.3	0.19	0.17	0.15	0.06
/Py_{nd}Saf	**Zn**	**Te**	**Au**	**Ag**	**Pb**	**Bi**								
	0.05	0.04	0.02	0.01	0.01	0.002								

Many researchers have stated that metals migrate to organic-rich mudstone directly from seawater with a slight dilution of sediment [67–69]. In particular, recent studies [62], supported by isotope data on Cr, Mo and Os, provide firm evidence that metals migrated from seawater due to the oxidation weathering of the continental crust and accumulated in highly metalliferous organic-rich mudstone in the Yangtze Cambrian Basin (South China). In terms of a complex of chemical elements (Mo, Se, Ni, Zn, V and P), the studied black shales resemble both highly metalliferous deposits and "normal black shales" which lack trace element anomalies [27].

These of trace elements (Mo, Se, Ni, Zn, V, P) are bioessential and they are sources to the oceans primarily though oxidative weathering of the continents and surface runoff. However, these group of trace elements are not not typical of sedimentary–diagenetic pyrite of SEDEX Pb–Zn–Cu stratiform which is usually enriched with Tl, Mn, Zn, Cu, Pb, As and Sb, [56,70]. Zinc is the only element common to both systems, but its occurrence is not unambiguous evidence of a hydrothermal origin. Nevertheless, some HMBS samples from the Mecca Quarry shales (IL, USA) and the Lisburne Group (Nothern Alaska, USA) have extremely high contents of Zn, Cd, Ag and/or Tl that may be due to the addition of metals after sedimentation or their hydrothermal migration to seawater from distal sources [58,71].

Most researchers believe that organic matter in the highly metalliferous black shales is of biological origin [72], mainly as phytoplankton detritus, deposited from the photic zone. They have seen an important connection between this process and the enrichment of organic matter with metals. In our opinion, however, they ignore the possibility of an abnormal development of bacterial mats associated with seep activity. The development of gas seepage processes on the bottom of the West Siberian Sea during the Late Jurassic could have taken place in connection with rifting, although it is not yet proven. However, this idea is supported by evidence of the influence of CH_4 seepage on authigenic iron sulfide formation in a range of hypoxic to anoxic conditions in Cretaceous–Paleocene of the eastern part of West Siberian Sea where giant iron-oxide deposits were formed [49]. In the Bazhenov Formation, abundance of pyritized nodules with relict microbial mat-related laminated structures (MRS) are similar to MRS found in black shales of different ages [26].

The emergence of such mats, based on methanotrophic chemosynthesis could provide the observed uneven accumulation of organic matter in sediments of the Bazhenov Formation. Moreover, one can assume that there were zones of anomalous development of plankton (radiolarians) above

zones of bacterial chemosynthesis, where seawater was also in need of enrichment with nutrient chemical elements. It is not unlikely that the Bazhenov Formation resulted from a combination of fluid seepage and biogenic processes in contrast to the theory of background active erosion of the Ural Mountains. Many papers emphasise that methane seeps and methane oxidized bacteria produce microbial mats [73]. A possible oxic modern analogue is the coeval seepage of hydrothermal and organic-rich fluids in the Guaymas basin with black smokers, seeps and microbial mats associated with oil redistribution [74].

The distal hydrothermal genesis of metals in respect of the Bazhenov Formation has not yet been proven. In the Jurassic, after the Triassic calm period, the global events of pyrite formation, resulted in the formation of the Se-rich copper sulfide deposits took place in the Mediterranean, Cordillera and Caribbean pyrite-bearing belts [75–77]. However, epochs of sulfide ore formation were usually followed by epochs of formation of bituminous deposits with a span of a few million years between them. As a rule, the residence time of many metals in the ocean are short (<100 years) or long (millennia) [63]. Therefore, we cannot generalize the influence of all hydrothermal trace elements on geochemical composition of Bazhenov Formation.

Intensive hydrothermal alteration or proximal sulfides have not yet been recognized at the level of the Bazhenov Formation. One can suppose, of course, that there were diffuse fluid seepages on the sea floor, with which the formation of bacterial mats–potential oil sources were associated. The development of sulfide-forming organic-rich seepages, surrounded by biotic assemblages, occurred during the Jurassic in the Middle Russian Sea (Tarkhany locality, Kazan area) [78]. However, the enrichment of pyrite with metals is not connected with such seepages, possibly due to low temperatures of mineral genesis.

The processes of erosion of the Ural Mountains, enclosing sulfide, iron, molybdenum–copper porphyry, gold, chromite, nickel and other deposits in the Mesozoic, could presumably supply adjacent marine basins with diverse bioessential chemical elements (Cu, Zn, Se, Mo, Cr, Ni, V and others), which are necessary for plankton to flourish with the formation of corresponding bituminous sediments as previously inferred [79]. Trace element redox-indicators and, first of all, Mo/Co and Se/Co suggest their formation under the conditions of higher oxygen content in the atmosphere [6,18,63]. It is suggested a cyclic distribution of Se and Se/Co in sedimentary–diagenetic pyrite across the Phanerozoic [38].

According to our data, the Bazhenov Formation of the Volgian Stage of the Upper Jurassic follows this tendency. A surprising combination of anoxic and euxinic conditions of sedimentation corresponding with peaks of oxygen concentration in the atmosphere is considered to be the main reason for the formation of this-type of highly metalliferous deposit. It would seem that the enrichment of sedimentary–diagenetic pyrite in Se and other trace elements is correlated with periods of plate-tectonic collision processes that, on the one hand, contributed to a supply of the sea biota with abundant nutrition [6] and, on the other hand, provide conditions for CH_4 seep formation favorable for bacterial chemosynthesis and forming of microbial mats as precursors of oil deposits.

Anoxic and euxinic conditions of bottom waters have constrained Co and Mn concentration in pyrite to low levels. These conditions are characterized by high enrichment of seafloor waters in Mo, Zn, Se and V [80,81]. The euxinic waters promote capture of Fe^{2+} and storage by the precipitation of sulfides, whereas Mn^{2+} and Co^{2+} are preserved in solution [11]. It is interesting that in our case framboidal pyrite is enriched in Mn which contradicts this statement.

In a first approximation, the epochs of sulfide ore formation in vast regions were followed by epochs of oil accumulation. This also relates to the change of Devonian sulfide-ore complexes of the Urals followed by oil-bearing complexes of the Domanik Formation [2]. It is obvious that rift-related volcanogenic settings were followed by accumulation of sedimentary deposits; the change of high-temperature sulfide ore-forming hydrothermal systems to organic-rich seepages in shallow-water seas followed the same tendency.

We assume that, by analogy with the Devonian cycle, there was the Triassic–Jurassic cycle, which included the formation of the North Sosva graben at the early stage. The latter is described in detail in a recent monograph [64]. Copper massive sulfide deposits have not been discovered so far

in the volcanogenic basement of the West Siberian megabasin, but one can assume their discovery will be with rift-related structures in deep-water areas. For example, younger cycles are known on Honshu Island, where the sulfide ore formation in the Miocene was followed by the deposition of oil-bearing sequences [82].

The subsequent history of the development of the Bazhenov Formation also seems promising. A part of this formation, obviously, entered into the zones of catagenetic and early metamorphic pyrrhotite transformation from pyrite—the process, which leads to the formation of gold deposits [18,83]. It makes sense that the Bazhenov bituminous shales, being in the tectonic fault zones, could be a source of formation of gold-ore deposits, since framboidal pyrite contains at least 0.1 ppm Au [18].

6. Conclusions

Framboidal and nodular pyrite are dominant varieties in the Bazhenov Formation. The large framboidal pyrite sizes and their cluster indicate that most have grown below the seafloor at the dysoxic-anoxic interface within organic-rich sediments, rather than in euxinic seawater columns. The dysoxic–anoxic conditions are supported by moderate values of the syngenetic pyrite index. The abundant barite in the black shales could be explained by excesses of Ba^{2+} and SO_4^{2-} formed highly likely due to early diagenetic decay of feldspar and oxidation of H_2S-rich seep fluids, respectively.

Some nodule-like pyritized bituminous layers and pyrite nodules with fine-grained laminated pyrite are similar by structure to pyritized microbial mat fragments. The microbial mats may have accumulated due to H_2S–CH_4 seepage providing massive bioproductivity by bacterial chemosynthesis. Coarse-grained pyrite in the nodules result from crystallization toward the end of early diagenesis.

Framboidal pyrite of the Bazhenov Formation is enriched in redox-sensitive elements such as Mo, V, Au, Cu, Pb, Ag, Ni, Se, and Zn in comparison with the host shales and nodular pyrite. Nodular pyrite has higher concentrations of As and Sb only. The trace element associations are characterized by strong positive correlations that can be interpreted as nano-inclusions of organic matter (Mo, V, Au), sphalerite (Zn, Cd, Hg, Sn, In, Ga, Ge), galena (Pb, Bi, Sb, Te, Ag, Tl) and tennantite (Cu, As, Sb, Bi, Te, Ag, Tl) in the pyrite studied. The substitution of Co, Ni, As and Sb into the pyrite lattice cannot be rejected. Many of the trace elements of the mineral inclusions, except sphalerite assemblage, show an inverse proportional relationship with V, suggesting a prior association with organic matter.

On the global scale, pyrite of the Bazhenov Formation is very similar to pyrite from highly metalliferous bituminous deposits, associated, as a rule, with gas and oil-and-gas deposits, which are characterized by higher Se and the complex of metals (Mo, Zn, Cu, Ni, Cd). In the Bazhenov Formation, the framboidal pyrites with high Mo, Zn, and Au and low Pb are in contrast with sedimentary-diagenetic pyrite (framboids, small crystals) from worldwide black shales barren of oil and gas. In general, the pyrite varieties from the Bazhenov Formation is characterized by high contents of Mo, Tl, Sb, Zn, Cu, Au and Ag in comparison with pyrite from gold–copper–iron skarn, porphyry copper–gold, and gold-ore orogenic deposits, being different from them in the extremely low contents of Co. The pyrite of SEDEX deposits are enriched in Pb, Ag, Co, Cu, Ni, Zn, Te and Tl and depleted in Mo in comparison with pyrite from the Bazhenov Formation. Enrichment with Mo and Sb indicate a higher influence of seawater during the formation of pyrite from the Bazhenov Formation in comparison to other styles of ore deposit presented herein

The most important criteria for evaluation of hydrothermal versus seawater metal sources come from our study of geochemical differences of the pyrite in VHMS deposits hosted by black shales compared with pyrite from the Bazhenov Formation. The pyrite of the Bazhenov Formation contains relative higher Cr, V, Ni, Mo, which is related to an oceanic water source. In contrast, the same pyrite varieties located in the black shales of Safyanovskoe VHMS deposit are enriched in heavy metals (Bi, Pb, Ag, Au, Te) indicating a variable temperature of initial hydrothermal concentration. Concentrations of transitional elements such as Zn and Cu in framboidal pyrite are similar in both deposit types. The framboidal pyrite formed in black shales of the Bazhenov Formation does not reflect any impact of fluids from a typical hydrothermal massive sulfide-forming system. The source

of Zn and Cu in the Bazhenov Formation could be massive sulfide deposits of the Urals Mountains weathered at the same Mesozoic time rather than some hydrothermal source of these elements. It is not improbable that the formation of the Bazhenov Formation has resulted from either a unique combination of the erosion of the Ural Mountains from one side and the simultaneous manifestation of organic-rich gas seep activity in the West Siberian Sea from another direction. It is suggested, that cold CH_4 seeps provided bacterial chemosynthesis of organic mats as scavengers of trace elements and became precursors of pyrite and oil deposits. This theory may explain the formation of bituminous deposits unique in reserves of oil, gas and metals.

Supplementary Materials: The following are available online at www.mdpi.com/2075-163X/10/5/449/s1, Table S1: Trace elements with correlation analysis in framboid pyrite Bazhenov Formation; Table S2: Trace elements with correlation analysis in nodular pyrite Bazhenov Formation.

Author Contributions: K.S.I., sampling and writing of the paper; V.V.M., writing of the paper and interpretation of the results; D.A.A., LA-ICP-MS analysis and formalization; A.S.T., preparation. All authors have read and agreed to the published version of the manuscript.

Funding: The study was funded by partly by Ministry of Science and Higher Education (State Contract No. AAAA-A18-118052590032-6 and AAAA-A19-119061790049-3).

Conflicts of Interest: The authors declare no conflict of interest.

References

1. Zanin, Y.; Zamirailova, A.G.; Eder, V.G. Chalcophile elements in black shales of the Bazhenov Formation, West Siberian sea basin. *Russ. Geol. Geoph.* **2016**, *57*, 608–616, doi:10.1016/j.rgg.2015.03.018.
2. Kanipova, Z.A.; Michurin, S.V.; Gorozhanin, V.M.; Velivetsckaya, T.A.; Ignatiev, A.V. Isotope-geochemical characteristic of the pyrite from oil-bearing beds in Ayaz oil deposit (Bashkirian Cis-Urals). In *Geological Digest # 11*; IG USC RAS: Ufa, Russia, 2014; pp. 169–175. (In Russian)
3. Berner, Z.A.; Puchelt, H.; Nöltner, T.; Kramar, U. Pyrite geochemistry in the Toarcian Posidonia Shale of southwest Germany: Evidence for contrasting trace-element patterns of diagenetic and syngenetic pyrites. *Sedimentology* **2013**, *60*, 548–573, doi:10.1111/j.1365-3091.2012.01350.
4. Pisarzowska, A.; Berner, Z.A.; Racki, G. Geochemistry of Early Frasnian (Late Devonian) pyrite-ammonoid level in the Kostomłoty Basin, Poland, and a new proxy parameter for assessing the relative amount of syngenetic and diagenetic pyrite. *Sediment. Geol.* **2014**, *308*, 18–31, doi:10.1016/j.sedgeo.2014.04.009.
5. McManus, J.; Berelson, W.B.; Severmann, S.; Poulson, R.L.; Hammond, D.E.; Klinkhammer, G.P.; Holm, C. Molybdenum and uranium geochemistry in continental margin sediments: paleoproxy potential. *Geochim. Cosmochim. Acta* **2006**, *70*, 4643–4662, doi:10.1016/j.gca.2006.06.1564.
6. Johnson, A.C.; Large, R.R.; Coveney, R.M.; Kelley, K.D.; Slack, J.F.; Steadman, J.A.; Gregory, D.D.; Sack, P.J. Secular distribution of highly metalliferous black shales corresponds with peaks in past atmosphere oxygenation. *Miner. Depos.* **2017**, *52*, 791–798, doi:10.1007/s00126-017-0735-7.
7. Tribovillard, N.; Algeo, T.J.; Baudin, F.; Riboulleau, A. Analysis of marine environmental conditions based on molybdenum–uranium covariation—Applications to Mesozoic paleoceanography. *Chem. Geol.* **2012**, *324–325*, 46–58, doi:10.1016/j.chemgeo.2011.09.009
8. Helz, G.R.; Vorlicek, T.P. Precipitation of molybdenum from euxinic waters and the role of organic matter. *Chem. Geol.* **2019**, *509*, 178–193, doi:10.1016/j.chemgeo.2019.02.001.
9. Smrzka, D.; Zwicker, J.; Bach, W.; Feng, D.; Himmler, T.; Chen, D.; Peckmann, J. The behavior of trace elements in seawater, sedimentary pore water, and their incorporation into carbonate minerals: a review. *Facies* **2019**, *65*, 25–47, doi:10.1007/s10347-019-0581-4.
10. Algeo, T.J.; Liu, J. A re-assessment of elemental proxies for paleoredox analysis. *Chem. Geol.* **2020**, *540*, in press, doi:10.1016/j.chemgeo.2020.119549.
11. Large, R.R.; Mukherjee, I.; Gregory, D.D.; Steadman, J.A.; Maslennikov, V.V.; Meffre, S. Ocean and atmospere geochemical proxies derived from trace elements in marine pyrite implication for ore genesis in sedimentary basins. *Econ. Geol.* **2017**, *12*, 423–450, doi:10.2113/econgeo.112.2.423.
12. Emsbo, P.; Hofstra, A.H.; Johnson, C.A.; Koenig, A.; Grauch, R.; Zhang, X.; Hu, R.; Su, W.; Pi, D. Lower Cambrian metallogenesis of south China: Interplay between diverse basinal hydrothermal fluids and marine chemistry. In *Mineral Deposit Research: Meeting the Global Challenge: Proceedings of the Eighth Biennial*

SGA Meeting Beijing, China, 18–21 August 2005; Springer Verlag: Berlin/Heidelberg, Germany, 2005; pp. 115–118.
13. Koski, R.A.; Stakes, D.S.; Lamothe, P.J.; Crock, J.G. Metal enrichments in hydrothermal petroleum from sediment-covered spreading counters, Northern Pacific Ocean. *GSA Abstracts* **2004**, *36*, 200.
14. Zhang, K.; Jiang, Z.; Yin, L.; Gao, Z.; Wang, P.; Song, Y.; Jia, C.; Liu, W.; Liu, T.; Xie, X.; et al. Controlling functions of hydrothermal activity to shale gas content taking lower Cambrian in Xiuwu Basin as an example. *Mar. Pet. Geol.* **2017**, *85*, 177–193, doi:10.1016/j.marpetgeo.2017.05.012.
15. Large, R.R.; Danyushevsky, L.; Hollit, C.; Maslennikov, V.; Meffre, S.; Gilbert, S.; Bull, S.; Scott, R.; Emsbo, P.; Thomas, H.; et al. Gold and trace element zonation in pyrite using a laser imaging technique: Implications for the timing of gold in orogenic and Carlin-style sediment-hosted deposits. *Econ. Geol.* **2009**, *104*, 635–668, doi:10.2113/gsecongeo.104.5.635.
16. Kiryukhina, T.A.; Fadeeva, N.P.; Stupakova, A.V.; Poludetkina, E.N.; Sautkin, R.S. Domanian deposits of the Timan-Pechora and Volga-Ural basins. *Geol. Oil Gas* **2013**, *3*, 76–87. (In Russian)
17. Danyushevsky, L.; Robinson, P.; Gilbert, S.; Norman, M.; Large, R.; McGoldrick, P.; Shelley, M. Routine quantitative multi-element analysis of sulphide minerals by laser ablation ICP–MS: Standard development and consideration of matrix effects. *Geochem. Explor. Environ. Anal.* **2011**, *11*, 51–60, doi:10.1144/1467-7873/09-244.
18. Large, R.R.; Bull, S.; Maslennikov, V.V. A carbonaceous sedimentary source-rock model for Carlin-type and orogenic gold deposits. *Econ. Geol*. **2011**, *106*, 331–358, doi:10.2113/econgeo.106.3.331.
19. Gregory, D.D.; Large, R.R.; Halpin, J.A.; Lounejeva, E.; Lyons, T.W.; Wu, S.; Danyushevsky, L.V.; Sack, P.; Chappaz, A.; Maslennikov, V.V. Trace element content of sedimentary pyrite in black shales. *Econ. Geol.* **2015**, *110*, 1389–1410, doi:10.2113/econgeo.110.6.1389.
20. Wilson, S.A.; Ridley, W.I.; Koenig, A.E. Development of sulphide calibration standards for the laser ablation inductively-coupled plasma mass spectrometry technique. *J. Anal. Atom. Spect.* **2002**, *17*, 406–409, doi:10.1039/B108787H.
21. Paton, C.; Hellstrom, J.; Paul, B.; Woodhead, J.; Hergt, J. Iolite: Freeware for the visualisation and processing of mass spectrometric data. *J. Anal. Atom. Spect.* **2011**, *26*, 2508–2518, doi:0.1039/c1ja10172b.
22. Smirnov, B.I. *Correlation Methods in Paragenetic Analysis*; Nedra: Moscow, Russia, 1981, p. 176. (In Russian)
23. Braduchan, Y.V.; Gurari, F.G.; Zakharov, V.A. *Bazhenov Horizon in West Siberia (Startigraphy, paleogeography, Ecosystem, and Oil-Bearing Capacity)*; Nauka: Novosibirsk, Russia, 1986; p. 217. (in Russian)
24. Ivanov, K.S.; Volkov, V.A.; Vakhrusheva, N.V. Paleogeography of the Bazhenov Formation based on the distribution of rare-earth elements. *Dokl. Earth Sci.* **2019**, *488*, 1094–1096, doi:10.1134/S1028334X19090150.
25. Amon, E.O. Radiolarians from the Bazhenov (Volgian Stage) Formation of latitudinal Ob River region, West Siberia, Western Siberia. In *Transactions of Institute of Geology and Geochemistry. Yearbook-2010*; IGiG UB RAS: Ekaterinburg, Russia, 2011; pp. 3–8. (In Russian)
26. Aubineu, J.; Abani, A.E.; Bekker, A.; Somogyi, A.; Bankole, O.M.; Macchiarelli, R.; Meunier, A.; Riboulleau, A.; Reynaud, J.-R.; Konhauser, K.O. Microbially induced potassium enrichment in Paleoproterozoic shales and implication for reverse weathering of early Earth. *Nat. Commun.* **2019**, *10*, 2670, doi:10.1038/s41467-019-10620-3.
27. Ketris, M.P.; Yudovich, Y.E. Estimations of clarkes for carbonaceous biolithes: World averages for trace element contents in black shales and coals. *Int. J. Coal Geol.* **2009**, *78*, 135–148, doi:10.1016/j.coal.2009.01.002.
28. Gavshin, V.M.; Zakharov, V.A. Geochemistry of the Upper Jurassic-Lower Cretaceous Bazhenov Formation, West Siberia. *Econ. Geol.* **1996**, *9*, 122–133. doi:10.2113/gsecongeo.91.1.122.
29. Volkov, E.N.; Smertina, L.N. Speciation of chalcophile elements in the rocks of the Bazhenov Formation. In *Association of Trace Elements with Organic Matter in the Sedimentary Sequences of Siberia*; Kuznetsov, V.A., Ed.; IGG SB RAS: Novosibirsk, Russia, 1984; pp. 32–40. (In Russian)
30. Wohlgemuth-Ueberwasser, C.C.; Viljoen, F.; Petersen, S.; Vorster, C. Distribution and solubility limits of trace elements in hydrothermal black smoker sulfides: An in-situ LA-ICP-MS study. *Geochim. Cosmochim. Acta* **2015**, *159*, 16–41, doi:10.1016/j.gca.2015.03.020.
31. D'yachkova, I.B.; Khodarkovskiy, I.L. Thermodynamic equilibria in the system S–H_2O, Se–H_2O and Te–H_2O in the 25–300 °C temperature range and their geochemical interpretation. *Geochem. Int.* **1968**, *5*, 1108–1125.
32. Cutter, G.A. Selenium in reducing waters. *Science* **1982**, *217*, 829–831, doi:10.1126/science.217.4562.829.

33. Seby, F.; Potin-Gautier, M.; Giffaut, E.; Borge, G.; Donard, O.F.X. A critical review of thermodynamic data for selenium species at 25 °C. *Chem. Geol.* **2001**, *171*, 173–194, doi:10.1016/S0009-2541(00)00246-1.
34. Bruggeman, C.; Maes, A.; Vancluysen, J.; Vandemussele, P. Selenite reduction in Boom clay: Effect of FeS_2, clay minerals, and dissolved organic matter. *Environ. Pollut.* **2005**, *137*, 209–221, doi:10.1016/j.envpol.2005.02.010.
35. Yudovich, Y.E.; Ketris, M.P. *Trace Elements in Black Shales*; Nauka: Ekaterinburg, Russia, 1994, p. 304. (In Russian)
36. Clarke, M.B.; Helz, G.R. Metal–thiometalate transport of biologically active trace elements in sulfidic environments. 1. Experimental evidence for copper thioarsenite complexing. *Environ. Sci. Technol.* **2000**, *34*, 1477–1482, doi:10.1021/es990134g.
37. Gordeev, V.V. *Geochemistry of the River–Sea System*; IP Matushkina: Moscow, Russia, 2012; p. 452. (In Russian)
38. Large, R.R.; Gregory, D.D.; Steadman, J.A.; Tompkins, A.G.; Lounjeva, E.; Danyushevsky, L.D.; Halpin, J.A.; Maslennikov, V.V.; Sack, P.J.; Mukherjee, I.; et al. Gold in the oceans through time. *Earth Planet. Sci. Lett.* **2015**, *428*, 139–150, doi:10.2113/econgeo.111.1.89.
39. Large, R.R.; Halpin, J.A.; Danyushevsky, L.V.; Maslennikov, V.V.; Bull, S.; Long, J.A.; Gregory, D.D.; Lounejeva, E.; Lyons, T.; Sack, P.J.; et al. Trace element content of sedimentary pyrite as a new proxy for deep-time ocean-atmosphere evolution. *Earth Planet. Sci. Lett.* **2014**, *389*, 209–220, doi:10.1016/j.epsl.2013.12.020.
40. Ivanov, V.V. *Ecological Geochemistry of Elements*; Nedra: Moscow, Russia, 1996. (In Russian)
41. Chappaz, A.; Lyons, T.W.; Gregory, D.D.; Reinhard, C.T.; Gill, B.C.; Li, C.; Large, R.R. Does pyrite act as an important host for molybdenum in modern and ancient euxinic sediments? *Geochem. Cosmochem. Acta* **2014**, *126*, 112–122, doi:10.1016/j.gca.2013.10.028.
42. Shevkunov, A.G.; Maslennikov, V.V.; Large, R.R.; Maslennikova, S.P.; Danyushevsky, L.V. Geochemical features of varieties of pyrite from the Kumtor gold-ore deposit, Kyrgyzstan. *Mineralogiya* **2018**, *4*, 22–40. (in Russian)
43. Large, R.R.; Maslennikov, V.V.; Robert, F.; Danyushevsky, L.V. Multistage sedimentary and metamorphic origin of pyrite and gold in the Giant Sukhoi Log deposit, Lena Gold Province, Russia. *Econ. Geol.* **2007**, *102*, 1233–1267, doi:10.2113/gsecongeo.102.7.1233.
44. Safina, N.P.; Maslennikov, V.V. Consequence of the mineral-forming process in clastogenic ores of Safyanovskoye copper massive sulfide ore deposit (the Middle Urals). *Zap. Min. Obshch.* **2008**, *137*, 61–75. (in Russian)
45. Safina, N.P.; Ayupova, N.R. Diagenetic bournonite in clastic ores of the Safyanovskoe copper-zinc massive sulfide deposit, the middle Urals. *Zap. Min. Obshch.* **2017**, *146*, 73–87. (In Russian)
46. Maslennikov, V.V.; Ayupova, N.R.; Herrington, R.J.; Danyushevskiy, L.V.; Large, R.R. Ferruginous and manganiferous haloes around massive sulphide deposits of the Urals. *Ore Geol. Rev.* **2012**, *47*, 5–41, doi:10.1016/j.oregeorev.2012.03.008.
47. Wilkin, R.T.; Barnes, H.L.; Brantley, S.L. The size distribution of framboidal pyrite in modern sediments: An indicator of redox conditions. *Geochem. Cosmochem. Acta* **1996**, *60*, 3897–3912, doi:10.1016/0016-7037(96)00209-8.
48. Wignall, P.B.; Newton, R. Pyrite framboid diameter as a measure of oxygen deficiency in ancient mudrocks. *Amer. J. Sci.* **1998**, *298*, 537–552.
49. Rudmin, M.; Baanerjee, S.; Abdulayev, E.; Ruban, A.; Filimonenko, E.; Lyapina, E.; Kasharov, R.; Mazurov, A. Ooidal ironstones in Meso-Cenozoic sequences in western Siberia: Assessment of formation processes and relationship with regional and global earth processes. *J. Palaeogeogr.* **2020**, *9*, 1–21, doi:10.1186/s42501-019-0049-z.
50. Wei, H.; Chen, D.; Wang, J.; Yu, H.; Tucker, E.M. Organic accumulation in the lower Chihsia Formation (Middle Permian) of South China: Constraints from pyrite morphology and multiple geochemical proxies. *Palaeogeogr. Palaeoclimatol. Palaeoecol.* **2012**, *353–355*, 73–86, doi:10.1016/j.palaeo.2012.07.005.
51. Xiong, Z.; Li, T.; Algeo, T.; Nan, Q.; Zhai, B.; Lu, B. Paleoproductivity and paleoredox conditions during late Pleistocene accumulation of laminated diatom mats in the tropical West Pacific. *Chem. Geol.* **2012**, *334*, 77–91, doi:10.1016/j.chemgeo.2012.09.044.
52. Emsbo, P.; Johnson, C.A. Formation of modern and Paleozoic stratiform barite at cold methane seeps on continental margins: Comment and Reply: Comment. *Geology* **2004**, *31*, 897–900, doi:10.1130/G19652.1.

53. Raiswell, R. Pyrite texture, isotopic composition and availability of iron. *Amer. J. Sci.* **1982**, *282*, 1244–1263, doi:10.2475/ajs.282.8.1244.
54. Roychoudhury, A.N.; Kostka, J.E.; Cappelen, P.V. Pyritization: A palaeoenvironmental and redox proxy revaluated. *Estuar. Coast. Shelf Sci.* **2003**, *57*, 1183–1193, doi:10.1016/S0272-7714(03)00058-1.
55. Cook, N.J.; Ciobanu, C.L.; Spry, P.G.; Voudouris, P. Participants of IGCP-486. Understanding gold-(silver)-telluride-(selenide) deposits. *Episodes* **2009**, *32*, 249–263, doi:10.18814/epiiugs/2009/v32i4/002.
56. Mukherjee, I.; Large, R. Application of pyrite trace element chemistry to exploration for SEDEX style Zn–Pb deposits, McArthur Basin, Northern Territory, Australia. *Ore Geol. Rev.* **2016**, *81*, 1249–1270, doi:10.1016/j.oregeorev.2016.08.004.
57. Fru, E.C.; Somogyi, A.; Albani, A.E.; Aubineau, J.; Robbins, L.J.; Lalonde, S.V.; Konhauser, K.O. The rise of oxygen arsenic sycling at ca. 2.48 Ga. *Geology* **2019**, *47*, 243–246, doi:10.1130/G45676.2.
58. Coveney, R.M.; Glascock, M.D. A review of the origins of metal-rich 320 Pennsylvanian black shales, central U.S.A., with an inferred role for basial 321 brines. *Appl. Geochem.* **1989**, *4*, 347–367, doi:10.1016/0883-2927(89)90012-7.
59. Loukola-Ruskeeniemi, K. Geochemical evidence for the hydrothermal origin 417 of sulphur, base metals and gold in Proterozoic metamorphosed black shales, Kainuu and Outokumpu areas, Finland. *Miner. Depos.* **1991**, *26*, 152–164, doi:10.1007/BF00195262.
60. Och, L.M.; Shields-Zhou, G.A.; Poulton, S.W.; Manning, C.; Thirlwall, M.F.; Li, D.; Chen, X.; Ling, H.F.; Osborn, T. Redox changes in Early Cambrian 435 black shales at Xiaotan section, Yunnan Province, South China. *Precambrian Res.* **2013**, *225*, 166–189, doi:10.1016/j.precamres.2011.10.005.
61. Lehmann, B.; Mao, J.W.; Li, S.R.; Zhang, G.D.; Zeng, M.G. Re-Os dating of polymetallic Ni–Mo–PGE–Au mineralization in Lower Cambrian black shales of South China and its geologic significance—A reply. *Econ. Geol.* **2003**, *98*, 663–665, doi:10.2113/gsecongeo.98.3.663.
62. Lehmann, B.; Frei, R.; Xu, L.; Mao, J. Early Cambrian black shale hosted Mo–Ni and V mineralization on the rifted margin of the Yangtze Platform China: Reconnaissance chromium isotope data and a refined metallogenic model. *Econ. Geol.* **2016**, *111*, 89–104, doi:10.2113/econgeo.111.1.89.
63. Large, R.R.; Mukherjee, I.; Gregory, D.; Steadman, J.; Corkey, R.; Danyushevsky, L.V. Atmosphere oxygen cycling through the Proterozoic and Phanerozoic. *Miner. Depos.* **2019**, *54*, 485–506, doi:10.1007/s00126-019-00873-9.
64. Ivanov, K.S.; Fedorov, Y.N.; Erokhin, Y.V.; Ponomarev, V.S. *Geological Structure of the Basement of Trans-Urals Part of the West Siberian Oil-and-Gas Megabasin*; IGG UB RAS: Ekaterinburg, Russia, 2016; p. 302. (In Russian)
65. Safina, N.P.; Melekestseva, I.Y.; Ayupova, N.R.; Maslennikov, V.V.; Maslennikova, S.P.; Artemyev, D.A.; Blinov, I.A. Authigenesis at the Urals massive sulfide deposits: Insight from pyrite nodules hosted in ore diagenites. *Minerals* **2020**, *10*, 193.
66. Maslennikov, V.V.; Ayupova, N.R.; Safina, N.P.; Tseluyko, A.S.; Melekestseva, I.Y.; Large, R.R.; Herrington, R.J.; Kotlyarov, V.A.; Blinov, I.A.; Maslennikova, S.P.; et al. Mineralogical features of ore diagenites in the Urals massive sulfide deposits, Russia. *Minerals* **2019**, *3*, 150.
67. Delian, F.; Jie, Y.; Tiebing, L. Black shale series-hosted silver-vanadium deposits of the upper Sinian Doushantuo Formation, Western Hubei Province, China. *Explor. Min. Geol.* **1992**, *1*, 29–38.
68. Holland, H.D. Metals in black shales: A reassessment. *Econ. Geol.* **1979**, *74*, 1676–1680, doi:10.2113/gsecongeo.74.7.1676.
69. Kontinen, A.; Hanski, E. The Talvivaara black shale-hosted Ni–Zn–Cu–Co deposit in eastern Finland. In *Mineral Deposits of Finland*; Maier, W.A., Lahtinen, R., O'Brien, H., Eds.; Elsevier: Amsterdam, The Netherlands, 2015; pp. 557–612.
70. Lode, S.; Piercey, S.J.; Devine, C.A. Geology, mineralogy, and lithogeochemistry of metalliferous mudstones associated with the Lemarchant volcanogenic massive sulfide deposit, Tally Pond belt, central Newfoundland. *Econ. Geol.* **2015**, *110*, 1835–1859, doi:10.2113/econgeo.110.7.1835.
71. Slack, J.F.; Selby, D.; Dumoulin, J.A. Hydrothermal, biogenic, and seawater components in metalliferous black shales of the Brooks Range, northern Alaska: Synsedimentary metal enrichment in a carbonate ramp setting. *Econ. Geol.* **2015**, *110*, 653–675, doi:10.2113/econgeo.110.3.653.
72. Jenkyns, H.C. Geochemistry of oceanic an-oxic events. *Geochem. Geophis. Geosyst.* **2010**, *11*, Q03004, doi:10.1029/2009GC002788.

73. Paul, B.G.; Ding, H.; Bagby, S.C.; Kellermann, M.Y.; Redmond, M.C.; Andersen, G.L.; Valentine, D.L. Methane-oxidizing bacteria shunt carbon to microbial mats at a marine hydrocarbon seep. *Front. Microbiol.* **2017**, *8*, 186, doi:10.3389/fmicb.2017.00186.
74. Geilert, S.; Hensen, C.; Schmidt, M.; Liebetrau, V.; Scholz, F.; Doll, M.; Deng, L.; Fiskal, A.; Lever, M.A.; Su, C.C.; et al. On the formation of hydrothermal vents and cold seeps in the Guaymas Basin, Gulf of California. *Biogeosciences* **2018**, *15*, 5715–5731, doi:10.5194/bg-15-5715-2018.
75. Ivanov, S.N.; Bogdanova, E.I.; Kuritsina, N.A. (Eds.) *Copper Sulfide Deposits of Foreign Countries*; Nauka: Moscow, Russia, 1984; p. 216. (In Russian)
76. Borodaevskaya, M.B.; Gorzhevskii, A.I.; Krivtsov, A.I.; Ruchkin, G.V.; Skripchenko, N.S.; Tvalchrelidze, G.A.; Yakovlev, G.F. (Eds.) *Copper Sulfide Deposits of the World*; Nedra: Moscow, Russia, 1979; p. 284. (In Russian)
77. Kontar, E.S. Quantitative evaluation of massive sulfide ore formation. *Geol. Ore Depos.* **2002**, *44*, 543–555.
78. Nikolaeva, V.M.; Shilovskii, O.P.; Korolev, E.A. Morphological features of pyrite nodules form Middle Jurassic deposits. In *Metallogeny of Ancient and Modern Oceans–2014*; IMin UB RAS: Miass, Russia, 2014; pp. 76–79. (In Russian)
79. Robbins, L.J.; Lalonde, S.V.; Planavsky, N.J.; Partin, C.A.; Reinhard, C.T.; Krendall, B.; Scott, C.; Hardisty, D.S.; Gill, B.C.; Alessi, D.S.; et al. Trace elements at the intersection of marine biological and geochemical evolution. *Earth Sci. Rev.* **2016**, *163*, 323–348, doi:10.1016/j.earscirev.2016.10.013.
80. Brumsack, H.-J. The trace metal content of recent organic carbon-rich sediments: Implications for Cretaceous black shale formation. *Palaeogeog. Palaeoclimat. Palaeoecol.* **2006**, *232*, 344–361, doi:10.1016/j.palaeo.2005.05.011.
81. Tribovillard, N.; Algeo, T.J.; Lyons, T.; Riboulleau, A. Trace metals as paleoredoxand paleoproductivity proxies: An update. *Chem. Geol.* **2006**, *232*, 12–32, doi:10.1016/j.chemgeo.2006.02.012.
82. Glasby, G.P.; Yamanaka, T.; Yamamoto, J.; Sato, H.; Notsu, K. Kuroko and hydrocarbon deposits from Northern Honshu, Japan: A possible common hydrothermal/magmatic origin? *Resour. Geol.* **2004**, *54*, 413–424, doi:10.1111/j.1751-3928.2004.tb00217.x.
83. Thomas, H.V.; Large, R.R.; Bull, S.W.; Maslennikov, V.V.; Berry, R.F.; Fraser, R.; Froud, S.; Moye, R. Pyrite and pyrrhotite textures and composition in sedimentary rocks, laminated quartz veins, and gold reefs, at Bendigo Mine, Australia: Insights for ore genesis. *Econ. Geol.* **2011**, *105*, 1–40, doi:10.2113/econgeo.106.1.1.